Article

Neuron

Endogenous Gαq-Coupled Neuromodulator Receptors Activate Protein Kinase A

Highlights

- Activation of hippocampal muscarinic acetylcholine receptors increases PKA activity
- Gαq signaling is sufficient and necessary for this regulation
- The regulation is mediated by parallel signaling via either Ca^{2+} or PKC
- Activation of PKA occurs with many endogenous and designer Gαq-coupled receptors

Authors

Yao Chen, Adam J. Granger, Trinh Tran, Jessica L. Saulnier, Alfredo Kirkwood, Bernardo L. Sabatini

Correspondence

bernardo_sabatini@hms.harvard.edu

In Brief

Chen et al. show that hippocampal Gαq-coupled muscarinic receptors activate PKA, an effector classically associated with the Gαs/Gαi pathways. The regulation is mediated by parallel signaling via either Ca^{2+} or PKC and generalizes to other endogenous and designer Gαq-coupled receptors.

Chen et al., 2017, Neuron *96*, 1070–1083
December 6, 2017
https://doi.org/10.1016/j.neuron.2017.10.023

CellPress

CellPress

Neuron
Article

Endogenous Gαq-Coupled Neuromodulator Receptors Activate Protein Kinase A

Yao Chen,[1] Adam J. Granger,[1] Trinh Tran,[2] Jessica L. Saulnier,[1] Alfredo Kirkwood,[2] and Bernardo L. Sabatini[1,3,*]
[1]Department of Neurobiology, Howard Hughes Medical Institute, Harvard Medical School, 220 Longwood Avenue, Boston, MA 02115, USA
[2]Mind/Brain Institute, John Hopkins University, Baltimore, MD 21218, USA
[3]Lead Contact
*Correspondence: bernardo_sabatini@hms.harvard.edu
https://doi.org/10.1016/j.neuron.2017.10.023

SUMMARY

Protein kinase A (PKA) integrates inputs from G-protein-coupled neuromodulator receptors to modulate synaptic and cellular function. Gαs signaling stimulates PKA activity, whereas Gαi inhibits PKA activity. Gαq, on the other hand, signals through phospholipase C, and it remains unclear whether Gαq-coupled receptors signal to PKA in their native context. Here, using two independent optical reporters of PKA activity in acute mouse hippocampus slices, we show that endogenous Gαq-coupled muscarinic acetylcholine receptors activate PKA. Mechanistically, this effect is mediated by parallel signaling via either calcium or protein kinase C. Furthermore, multiple Gαq-coupled receptors modulate phosphorylation by PKA, a classical Gαs/Gαi effector. Thus, these results highlight PKA as a biochemical integrator of three major types of GPCRs and necessitate reconsideration of classic models used to predict neuronal signaling in response to the large family of Gαq-coupled receptors.

INTRODUCTION

Neuromodulators, such as acetylcholine, serotonin, and adrenaline, have profound effects on neural circuits and behavior. On a cellular level, these neuromodulators activate G-protein-coupled receptors (GPCRs), which transduce these extracellular signals into changes in the biochemical and electrical state of cells (Lefkowitz, 2007). Thousands of GPCRs encoded in mammalian genomes converge onto ~20-Gα proteins that fall into four major classes. The class identity of the specific Gα protein coupled to each receptor determines which of several distinct signaling pathways are activated upon ligand binding and therefore is used to predict the function of the GPCR (Gilman, 1995; Lefkowitz, 2007).

One of the most important signaling effectors of neuromodulator GPCRs is protein kinase A (PKA) (Dunn and Feller, 2008; Greengard, 2001; Williams et al., 2001). Classically, Gαs- and Gαi-coupled GPCRs up- and downregulate adenylyl cyclase activity, respectively, thereby controlling rates of production of cyclic AMP (cAMP), which activates PKA (Gilman, 1995). This push-pull control of PKA activity bidirectionally regulates numerous physiological processes in the nervous system, including transcription, synaptic transmission, synaptic plasticity, calcium influx, and learning (Drain et al., 1991; Higley and Sabatini, 2010; Kandel and Abel, 1995; Seol et al., 2007; Shen et al., 2008; Skeberdis et al., 2006; Skoulakis et al., 1993; Williams et al., 2001; Zhong et al., 2009).

Despite the importance of PKA for cellular physiology and animal behavior, our understanding of what neuromodulator inputs converge on PKA is incomplete. Notably, although Gαs/Gαi-coupled receptors clearly regulate PKA, whether Gαq-coupled receptors signal to PKA remains unclear. Classically, Gαq-coupled receptors signal to phospholipase C (PLC), and not PKA (Gilman, 1995; Hokin and Hokin, 1953). Based on the specificity of Gαq coupling and the selective modulation of downstream signaling pathways, Gαq-coupled designer receptors have been broadly used to increase neuronal excitability, since PLC-mediated depletion of phosphatidylinositol 4,5-bisphosphate (PIP2) leads to closure of K^+ channels (Airan et al., 2009; Armbruster et al., 2007; Guettier et al., 2009; Spangler and Bruchas, 2017; Sternson and Roth, 2014). Consequently, the effects of using Gαq-coupled designer receptors gated by light or exogenous small molecules are typically interpreted as resulting from manipulations of these classic Gαq effectors and not PKA.

The widely held assumption of the selectivity of Gαq signaling seems at odds with the reported crosstalk from Gαq-coupled receptors to the adenylyl cyclase/cAMP/PKA module (Bandrowski et al., 2001; Baumgold and Fishman, 1988; Burford et al., 1995; Olianas and Onali, 1992; Stein et al., 1988; Wang et al., 2008). Crosstalk can occur via direct coupling of Gαq-coupled receptors to Gαs or Gαi proteins (Burford and Nahorski, 1996; Masuho et al., 2015; Olianas and Onali, 1992; Stein et al., 1988), or in principle via the intracellular effectors of the Gαq pathways (Cooper et al., 1995; Geoffroy et al., 1999; Hunter et al., 2009; Lee et al., 1994; Lustig et al., 1993; Shen et al., 2012; Yoshimasa et al., 1987). However, for several reasons, the conclusions of these studies are insufficient to predict the effect of a specific, endogenously expressed Gαq-GPCR on PKA. First, different studies have reported that Gαq-coupled receptors increase, decrease, or do not change cAMP level/PKA activity, making it impossible to form a conclusion about the signaling downstream of a given GPCR. Second, although some intracellular effectors could *potentially* link a Gαq-GPCR to PKA based on studies in different

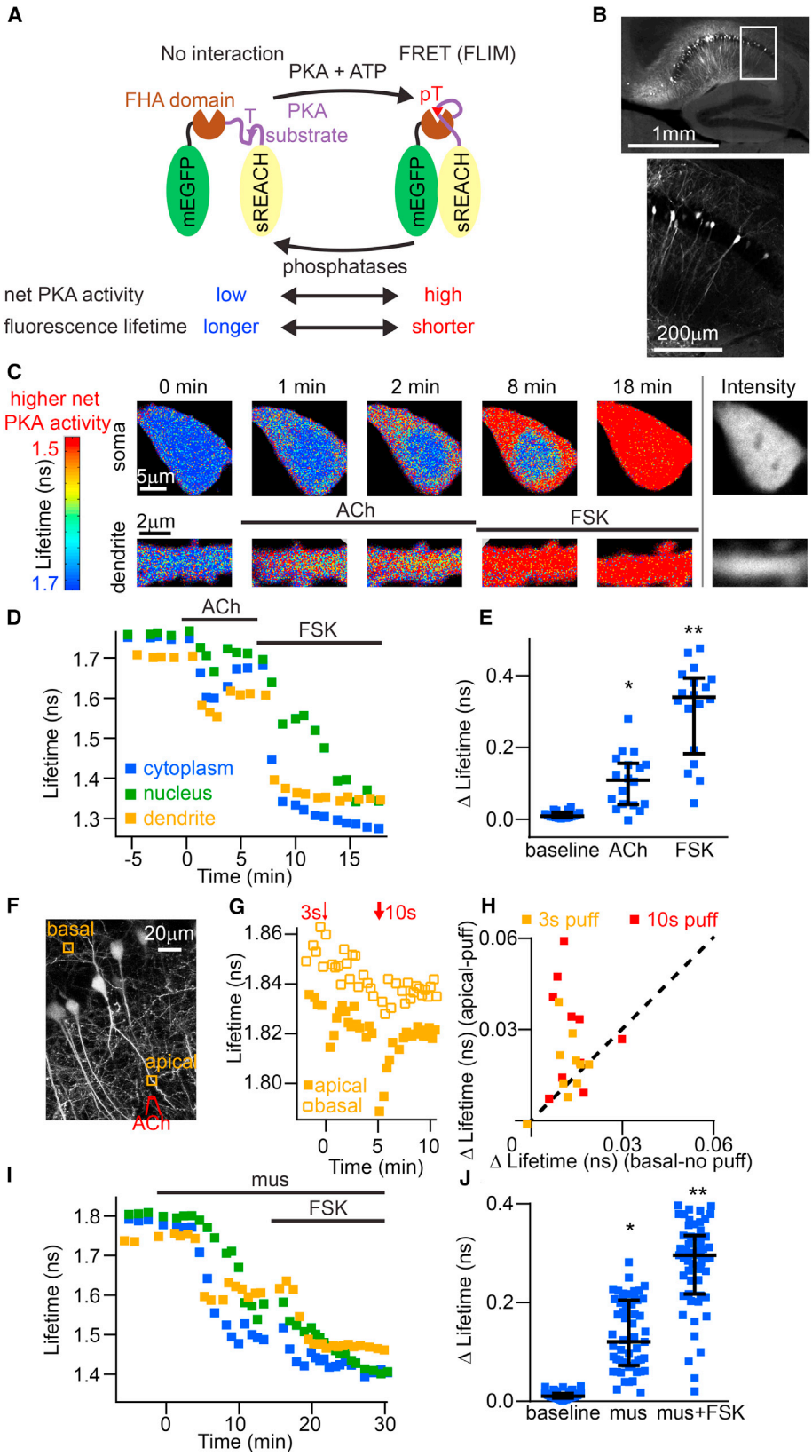

(legend on next page)

cells and systems, the Gαq-GPCR may not *actually* regulate PKA in a given system because the receptor, the intracellular effector, and PKA may be anchored in different subcellular compartments or microdomains (Gray et al., 1998; Lur and Higley, 2015; Tsvetanova and von Zastrow, 2014; Zhang et al., 2013). Third, many of these studies examined overexpressed receptors in heterologous systems, which often behave in qualitatively different ways to endogenous systems, because the nature of GPCR signaling is highly dependent on the expression level of GPCRs and their signaling effectors. Thus, it remains unclear whether endogenous Gαq-coupled receptors signal to PKA in the native brain, nor is it known in what context and cell types Gαq signaling regulates PKA activity.

Here, we examine the potential signaling to PKA by endogenous Gαq-coupled muscarinic acetylcholine receptors (mAChRs). PKA and mAChRs have each been identified as powerful regulators of synaptic plasticity, and their activity within the hippocampus promotes learning and memory (Brandon et al., 1997; Hasselmo, 2006; Higley and Picciotto, 2014; Seol et al., 2007; Skeberdis et al., 2006; Wess, 2004; Zhong et al., 2009). Two classes of mAChRs are expressed in the hippocampus: the Gαi-coupled mAChRs are expected to inhibit PKA, whereas the Gαq-coupled mAChRs are not classically predicted to signal to PKA (Caulfield, 1993; Hulme et al., 1990; Levey et al., 1995; Tice et al., 1996; Vilaró et al., 1990). Understanding whether endogenous Gαq-coupled mAChRs signal to PKA will provide insight into the normal physiology of this highly conserved receptor family, the mechanisms of action of cholinergic drugs that are widely used to treat neuropsychiatric disorders (Higley and Picciotto, 2014; Thathiah and De Strooper, 2009), and help with the prediction of cellular signaling and functions of the large family of Gαq-coupled receptors.

We use two-photon fluorescence lifetime imaging microscopy (2pFLIM) (Yasuda, 2006) and optical reporters of PKA activity that enable real-time analysis of endogenous GPCR signaling in acute hippocampal slices (Chen et al., 2014). We found that, in hippocampal neurons, mAChR activation enhances phosphorylation by PKA. In addition, Gαq signaling is both sufficient and necessary for this unusual neuronal regulation of a classic Gαs effector. Mechanistically, we revealed that mAChRs increase phosphorylation by PKA through parallel signaling via either Ca^{2+} transients or PKC activation, mechanisms likely shared by the large family of Gαq-coupled neuromodulator receptors. Indeed, Gαq-dependent elevation of net PKA activity is induced by both multiple endogenous receptors and widely used Gαq-coupled designer receptors. Given the critical role of PKA in cellular physiology, circuit processing, and animal behavior, our findings enhance our ability to understand and predict cellular signaling and physiological function of the large family of Gαq-coupled receptors.

RESULTS

mAChR Activation Increases Phosphorylation by PKA

In order to monitor PKA activity, we used our recently developed PKA activity sensor that allows quantitative real-time analysis of endogenous GPCR signaling with subcellular resolution in complex brain tissue (Chen et al., 2014). PKA activity was reported by FLIM-AKAR, a PKA substrate and a Förster resonance energy transfer (FRET)-based optical reporter that we engineered for optimal 2pFLIM (Figure 1A). Upon phosphorylation by PKA, the PKA substrate consensus region of FLIM-AKAR binds to the phosphopeptide binding domain, increasing FRET between the donor and acceptor fluorophores and decreasing donor fluorescence lifetime. Thus, FLIM analysis of FLIM-AKAR provides a quantitative measurement of its phosphorylation status, which reflects the net activity of PKA and its phosphatases (we subsequently refer to this, for simplicity, as net PKA activity). In contrast to many other methods, this approach allows the real-time monitoring of PKA phosphorylation downstream of endogenous GPCRs with native signaling cascades. We targeted FLIM-AKAR to the hippocampus via *in utero* electroporation and observed robust expression in hippocampal pyramidal neurons (Figure 1B).

To assess the effect of acetylcholine (ACh) on net PKA activity, we measured the fluorescence lifetime of FLIM-AKAR in CA1 pyramidal neurons in acute hippocampal slices using 2pFLIM. Tetrodotoxin (1 μM) was used in all experiments to block action

Figure 1. An Optical FRET-FLIM Reporter Reveals Net PKA Activation by Muscarinic Receptors in the Hippocampus

(A) Schematic of the PKA activity reporter FLIM-AKAR. Upon phosphorylation of the threonine residue (shown as T for before and pT for after phosphorylation) by PKA, the substrate region binds the FHA phosphopeptide binding domain. This brings the donor and acceptor fluorophores together, resulting in FRET and decreased donor fluorescence lifetime.

(B) Image of an acute brain slice expressing FLIM-AKAR in hippocampal CA1 and subiculum (top) with the boxed region illustrating soma and dendritic branches of CA1 neurons shown enlarged (bottom).

(C) Heatmap of FLIM-AKAR lifetime in a hippocampal CA1 neuron (top, soma; bottom, primary apical dendrite), in response to acetylcholine (ACh, 100 μM) and subsequent forskolin (FSK, 50 μM) application. On the right are fluorescence intensity images to illustrate morphology.

(D) The time course of net PKA activity in three subcellular compartments of the neuron in (C) during application of ACh and FSK.

(E) Summaries of lifetime changes in the somatic cytoplasm during baseline, and in response to ACh and FSK (*$p < 0.05$ versus baseline; **$p < 0.05$ versus ACh).

(F) Image with maximal projection of a z stack in the hippocampal CA1 region that shows the design of the ACh puffing experiment: ACh was puffed via a patching pipette (shown in red) onto an apical dendrite of a CA1 pyramidal neuron expressing FLIM-AKAR in acute hippocampal slices, and both apical and basal dendrites (imaged regions shown in the rectangles) were monitored for FLIM-AKAR lifetime change.

(G) The time course of net PKA activity in apical and basal dendrites of the neuron imaged in (F) in response to 3 and 10 s ACh (200 μM) puffs.

(H) X-Y summary plots of lifetime changes in the apical versus basal dendrites in response to 3 or 10 s ACh puffs.

(I) As in (D) for a representative neuron during application of muscarine (mus, 10 μM) and FSK.

(J) As in (E) in response to mus and subsequent FSK addition (*$p < 0.05$ versus baseline; **$p < 0.05$ versus mus). The composite data include stand-alone data as well as control datasets presented in other figures of this paper.

Each square represents a data point and black lines show median values with interquartile intervals. (B) and (F) were stitched from multiple images. See also Figure S1 and Table S1.

potentials. Surprisingly, ACh (100 μM) rapidly increased phosphorylation by PKA (as shown by a decrease in lifetime) in the somatic cytoplasm and dendrites (Figures 1C–1E and S1A–S1C; Table S1; cytoplasm, n = 18, p < 0.0001 for baseline versus ACh; dendrites, n = 7, p = 0.016). The nucleus also showed a clear, but slower, response (n = 18, p = 0.0001). Subsequent addition of forskolin (FSK, 50 μM) to directly activate ACs and increase PKA activity further decreased fluorescence lifetime (cytoplasm, n = 18, p < 0.0001 for ACh versus FSK; nuclei, n = 18, p < 0.0001; dendrites, n = 7, p = 0.016) and was used as a positive control for cell health and responsiveness to adenylyl cyclase (AC) activation in all experiments.

In order to mimic localized and transient ACh release *in vivo*, we puffed ACh (200 μM) onto apical dendrites with comparable temporal durations to ACh release measured in behaving mice (Figure 1F) (Parikh et al., 2007). Net PKA activity increased transiently in stimulated dendrites, with larger responses to 10 s than 3 s exposures (Figures 1G and 1H; n = 10, p = 0.014 for baseline versus 10 s). In contrast, no response was observed in the unstimulated basal dendrite of the same neuron (n = 10, p = 0.32 for baseline versus 10 s), which can respond when directly exposed to ACh (Figure S1D). Thus, ACh increases phosphorylation by PKA with spatial and temporal precision.

We hypothesized that activation of the G-protein-coupled ACh receptors, mAChRs, is sufficient to increase net PKA activity. Indeed, muscarine (mus, 10 μM) application reduced lifetime in all three subcellular compartments (Figures 1I–1J, S1E, and S1F; cytoplasm, n = 55; nuclei, n = 55; dendrites, n = 16; p < 0.0001 for all for baseline versus mus). Strikingly, the amplitude of the lifetime change in response to mus is similar to that in response to the Gαs-coupled β-adrenergic receptor agonist isoproterenol (iso) (Figures S2A and S2B). Interestingly, most cells showed a sustained lifetime decrease to mus and a transient lifetime decrease to iso. Finally, mus-induced FLIM-AKAR phosphorylation was abolished in the presence of the mAChR antagonist scopolamine (10 μM) (Figures S2E and S2F; n = 17; p = 0.58 for baseline versus mus [cytoplasm], p = 0.43 [nucleus]), confirming the specificity of mus to mAChRs. Thus, mAChR activation is sufficient to increase phosphorylation by PKA.

The specificity for PKA of the reporter's response was examined in two different ways. First, mAChR-induced FLIM-AKAR phosphorylation was significantly reduced by expression of a reporter with a point mutation (mut) that renders it not phosphorylatable by PKA (Figures 2A–2C and S3A) (cytoplasm and nuclei, n = 8 wild-type [WT], n = 14 [mut], p < 0.0001 for WT versus mut in both compartments; dendrites, n = 4 [WT], n = 7 [mut], p = 0.024). This indicates that the phosphorylatable residue is required for mAChR-induced reporter response. Second, expression of the PKA inhibitor PKI (Dalton and Dewey, 2006; Walsh et al., 1971), which is excluded from the nucleus (Wen et al., 1995), significantly reduced mAChR-induced FLIM-AKAR phosphorylation (cytoplasm, n = 16 [without PKI], n = 17 [with PKI], p = 0.0006 for without versus with PKI; dendrites, n = 10 [without PKI], n = 12 [with PKI], p = 0.0001) (Figures 2D–2F), yet cell health was unaffected as indicated by the electrical properties of the neurons (Figure S3B). Thus, PKA activity is required for mAChR-induced reporter response.

To further test the conclusion that net PKA activity increases in response to mAChRs, we developed a second method to measure activation of PKA that is independent from and orthogonal to FLIM-AKAR. This FRET-based optical reporter, PSI (for PKAc-substrate interaction), directly measures the physical interaction of PKA catalytic subunit (PKAc) with a substrate (Figure 2G). PSI consists of two molecules: (1) PKAc fused with monomeric enhanced GFP (mEGFP) (Zhong et al., 2009), which is excluded from the nucleus, and (2) monomeric cherry protein (mCherry) fused with a consensus region of PKA substrates with a point mutation that renders the substrate not phosphorylatable. Upon elevation of cAMP, PKAc-mEGFP is liberated from the regulatory subunits of PKA and binds to the mCherry-tagged PKA substrate, leading to FRET. Thus, PSI reports activation of PKA by monitoring the interaction between PKAc and its substrates, whereas FLIM-AKAR reports phosphorylation by endogenous PKA, making them independent methods of monitoring PKA activation. In response to mus, the PSI reporter showed increased FRET (Figures 2H and 2I; n = 11, p = 0.0098 for baseline versus mus), demonstrating that mus induces the interaction between PKAc and the substrate. Therefore, results from the two orthogonal optical sensors indicate that mus activates PKA.

Since the PKA response is qualitatively similar in all subcellular compartments, we focus our report on the somatic cytoplasm and include nuclear data in the supplemental figures.

Gαq-Coupled mAChR Activation Increases Net PKA Activity

Gαi-coupled GPCRs inhibit PKA activity, yet we observed increased net PKA activity in response to mus. Therefore, we hypothesized that Gαq-coupled mAChRs are sufficient to increase net PKA activity. We tested this hypothesis by activating endogenous Gαq-coupled M1 mAChRs (M1Rs) with the specific agonist 77-LH-28-1 (LH) (Langmead et al., 2008). Application of LH (10 μM) induced a large decrease in reporter lifetime to a similar degree as mus (Figures 3A, 3B, S4A, and S4B; n = 13, p = 0.0007 for baseline versus LH). Furthermore, LH-induced FLIM-AKAR phosphorylation was abolished in the presence of the mAChR antagonist scopolamine (10 μM) (Figures S2G and S2H; n = 9, p = 0.36 for baseline versus LH), confirming the selectivity of LH to mAChRs. These experiments reveal that activation of Gαq-coupled mAChRs is sufficient to enhance PKA phosphorylation in the hippocampus.

Such signaling from M1Rs to PKA may contribute to previously described but mechanistically poorly understood contributions of PKA to mAChR-dependent synaptic plasticity in pyramidal neurons (Dickinson et al., 2009; Jo et al., 2010; Seol et al., 2007). Indeed, inclusion of PKI in the recording pipette prevented M1R-induced synaptic depression (Figure S5; control, n = 11, p = 0.0020 for baseline versus LH; PKI, n = 12, p = 0.23 for baseline versus LH; p = 0.0070 for control versus PKI after LH treatment). Thus, PKA activity is required for M1R-induced synaptic depression, providing functional implications of our finding.

In principle, Gαq-coupled receptors may increase net PKA activity via Gαq signaling, or by promiscuous coupling to Gαs. Therefore, we used YM-254890 (YM), a specific inhibitor of the Gαq family of heterotrimeric G proteins ($G\alpha q/G_{11}/G_{14}$) (Nishimura et al., 2010), to test whether mus-induced increase in net

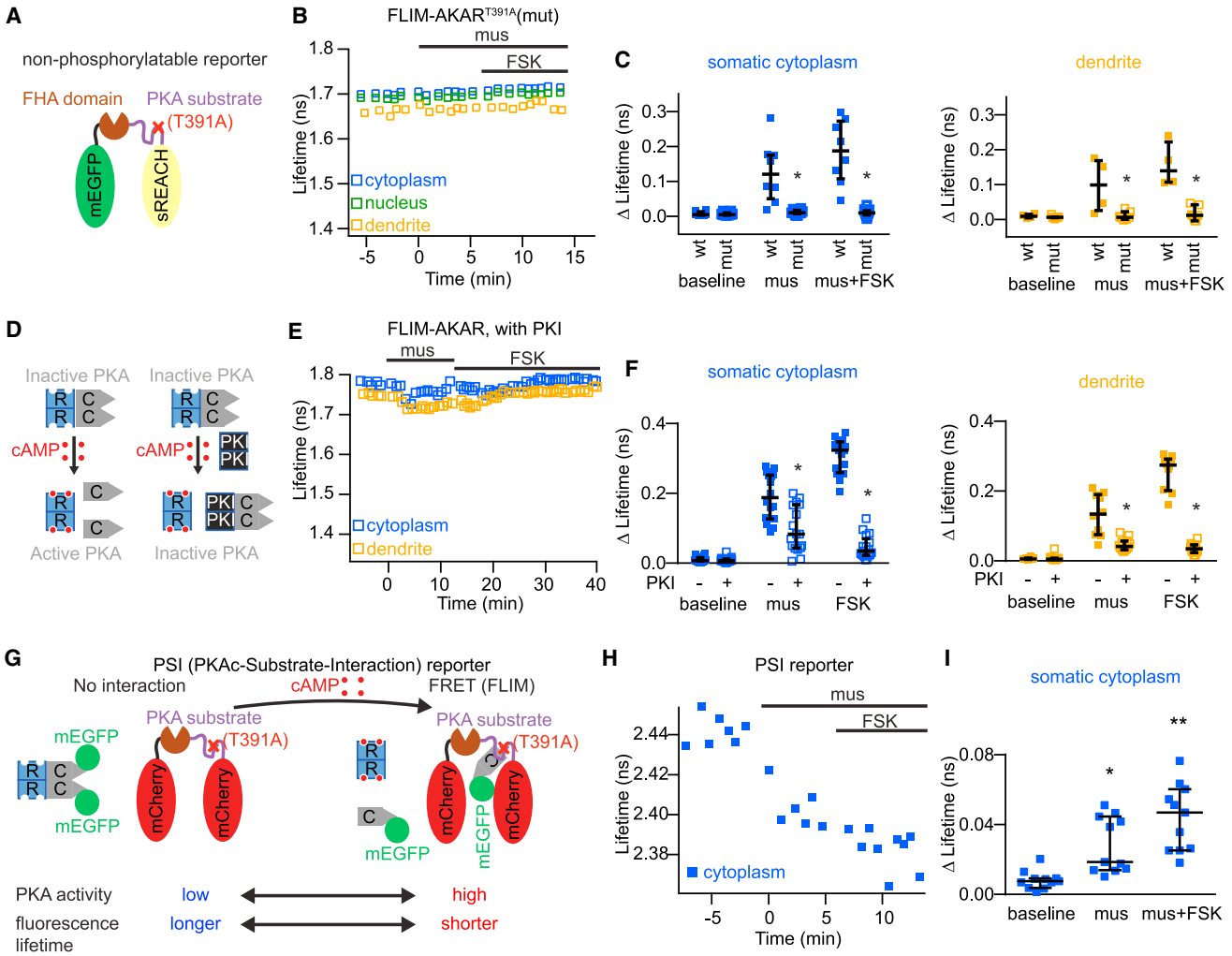

Figure 2. Specificity Controls for PKA and an Independent Reporter Validate Activation of PKA by Muscarinic Receptor Activation

(A) Schematic of the non-phosphorylatable reporter FLIM-AKAR^{T391A} in which the PKA phosphorylation site was mutated to alanine.

(B) Example plot showing FLIM-AKAR^{T391A} (mutant, abbreviated as mut) lifetime in CA1 neurons in response to 10 μM mus followed by 50 μM FSK in the somatic cytoplasm, nucleus, and dendrite.

(C) Summary plots showing the amplitudes of FLIM-AKAR or FLIM-AKAR^{T391A} lifetime changes in response to mus and FSK in the somatic cytoplasm and dendrite. *$p < 0.05$ versus WT.

(D) Schematic illustrating PKI inhibition of PKA. Binding of cAMP to the regulatory subunits (R) of PKA dissociates the regulatory and catalytic subunits (C), resulting in activation of PKA. PKI binds to the free catalytic subunits of PKA, thus inhibiting their activity.

(E) Example plots showing FLIM-AKAR response in the presence of PKI in response to mus followed by FSK in the cytoplasm and dendrite. Nucleus data were not shown because PKI is a nuclear excluded protein.

(F) Summary plots showing that PKI reduces the amplitudes of FLIM-AKAR lifetime changes in response to mus and FSK in the cytoplasm and dendrite. *$p < 0.05$ versus no PKI.

(G) Schematic of the PKAc-substrate interaction (PSI) reporter. Binding of cAMP to the regulatory subunits (R) of PKA liberates the catalytic subunits (C), which then bind to a consensus PKA substrate that has been mutated so that it is not phosphorylatable. The physical interaction between PKAc-mEGFP and substrate-mCherry brings the donor and acceptor fluorophores together, resulting in FRET and decreased donor fluorescence lifetime.

(H) Example plot showing PSI lifetime in CA1 neurons in response to 10 μM mus followed by 50 μM FSK in the somatic cytoplasm. Nucleus data were not shown because PKAc-mEGFP is excluded from the nucleus.

(I) Summary plot showing the amplitudes of PSI lifetime changes in response to mus and FSK in the somatic cytoplasm. *$p < 0.05$ versus baseline; **$p < 0.05$ versus mus.

Each square represents a data point and black lines show median values with interquartile intervals. See also Figures S2 and S3 and Table S1.

PKA activity requires Gαq signaling. Using the genetically encoded Ca^{2+} indicator GCaMP (Tian et al., 2009; Zariwala et al., 2012), we found that application of YM (1 μM) inhibited mus-induced Ca^{2+} transients, a signature of Gαq signaling, thus demonstrating the potency of the compound in acute hippocampal slices (Figures S2C and S2D; n = 7 for control, n = 6 for YM,

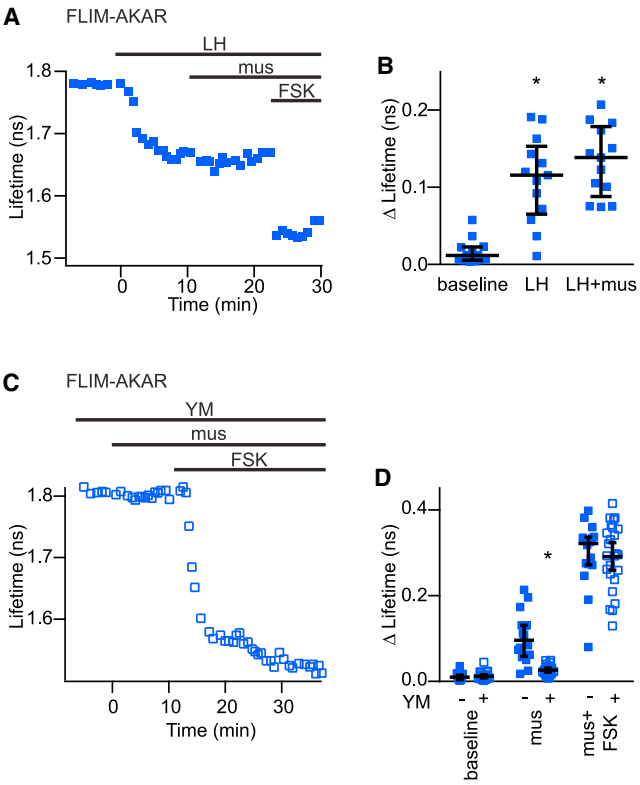

Figure 3. Gαq-Coupled Hippocampal mAChR Activation Increases Net PKA Activity

(A and B) Example plot (A) and summaries (B) showing modulation of net PKA activity by 77-LH-28-1 (LH, 10 μM), primarily an agonist of the Gαq-coupled M1 receptor, followed by application of mus and FSK. *p < 0.05 versus baseline.

(C and D) Example plot (C) and summaries (D) showing the effect on mus- and FSK-induced change in net PKA activity in the cytoplasm by an inhibitor of the $G\alpha q/G_{11}/G_{14}$ family, YM-254890 (YM, 1 μM). *p < 0.05 versus control

Each square represents a data point and black lines show median values with interquartile intervals. See also Figures S2 and S4–S6 and Table S1.

p = 0.0082 for control versus YM with mus). Furthermore, PKA activation in response to the activation of Gαs-coupled receptors remains intact in the presence of YM (Figures S2A and S2B; n = 5 for control, n = 8 for YM, p = 0.62 for control versus YM with iso), confirming that YM did not inhibit Gαs signaling. These positive and negative controls thus validate the utility of YM in determining the Gαq dependence of mus-triggered activation of PKA in our system. In HEK cells, PKA activation by overexpressed M1Rs was unaffected by YM application (Figure S6; n = 9, p = 0.0039 for baseline versus mus with YM), consistent with previous reports of Gαs coupling with overexpressed Gαq-GPCRs in heterologous systems (Burford and Nahorski, 1996). In contrast, YM significantly reduced endogenous mAChR-induced FLIM-AKAR phosphorylation in hippocampal CA1 pyramidal neurons (Figures 3C, 3D, S4C, and S4D; n = 16 for control, n = 25 for YM, p < 0.0001 for control versus YM with mus), indicating that signaling through the Gαq family is required for mus-induced increase in net PKA activity in the hippocampus. Furthermore, the contrasting results from HEK cells and the hippocampus demonstrate that what occurs endogenously is distinct from what occurs in a heterologous system, where overexpression likely induces artifactual crosstalk. Thus, endogenous Gαq-coupled receptors are sufficient to increase net PKA activity, and Gαq signaling is necessary for this regulation.

Ca^{2+} Transients Are Evoked, but Not Necessary, for mAChR-induced Net PKA Activity

To gain insight into the cell types and GPCRs that may display Gαq-mediated activation of PKA, we probed the mechanisms by which mAChRs modulate net PKA activity. Agonist binding to Gαq-coupled receptors activates PLCβ to cleave PIP2 into two second messengers: inositol triphosphate (IP_3) and diacylglycerol (DAG) (Berridge, 1983; Berridge et al., 1983; Kirk et al., 1981). IP_3 binding to its receptor leads to release of Ca^{2+} from intracellular stores; DAG or Ca^{2+} binds and activates PKC (Inoue et al., 1977; Streb et al., 1983; Takai et al., 1977) (Figure 4A). Thus, we investigated the involvement of the two branches of signaling pathways immediately downstream of PLC.

Since Ca^{2+}-activated ACs are expressed in the hippocampus (Cooper et al., 1995), we hypothesized that Ca^{2+} transients mediate mAChR-regulated net PKA activation. To determine conditions that inhibit mAChR-induced Ca^{2+} transients, we incubated slices in cyclopiazonic acid (CPA, 30 μM) to block Ca^{2+} loading into intracellular stores and used nominal 0 mM Ca^{2+} to minimize Ca^{2+} influx from the extracellular space (the combination is referred to as øCa^{2+} subsequently). This condition prevented mAChR-induced Ca^{2+} transients (Figures 4B–4D; n = 8 for control, n = 9 for øCa^{2+}; p = 0.0006 for control versus øCa^{2+} with mus).

Surprisingly, under the øCa^{2+} condition, the mAChR-induced decrease in FLIM-AKAR lifetime remained intact (Figures 4E, 4F, S7A, and S7B; n = 15 for control, n = 15 for øCa^{2+}; p = 0.80 for control versus øCa^{2+} with mus). Together, these experiments show that Ca^{2+} transients are evoked but Ca^{2+} alone is not necessary for mAChR-induced net PKA activation.

PKC Is Sufficient to Increase, but Not Necessary for, mAChR-induced Net PKA Activity

To probe the potential involvement of the second arm of Gαq signaling—activation of PKC—in mAChR-induced net PKA activation, we first examined whether PKC could non-specifically phosphorylate the reporter FLIM-AKAR. Consistent with previous results (Allen and Zhang, 2006), in HEK cells, application of phorbol 12,13-dibutyrate (PDBu, 1 μM), a DAG derivative that activates PKC, did not change FLIM-AKAR lifetime (Figure 5A; n = 12, p = 0.27 for baseline versus PDBu, p = 0.0005 for baseline versus FSK), indicating that PKC does not phosphorylate the reporter directly.

In the hippocampus, however, PDBu application robustly decreased reporter lifetime (Figures 5B, S7C, and S7D; n = 31, p < 0.0001 for baseline versus PDBu). This demonstrates that PKC activation is sufficient to increase net PKA activity in the hippocampus, but not HEK cells, revealing cell-type-specific regulation of PKA by PKC.

Biochemical evidence has demonstrated that PKC can phosphorylate adenylyl cyclase 2 (AC2) (Lustig et al., 1993; Shen

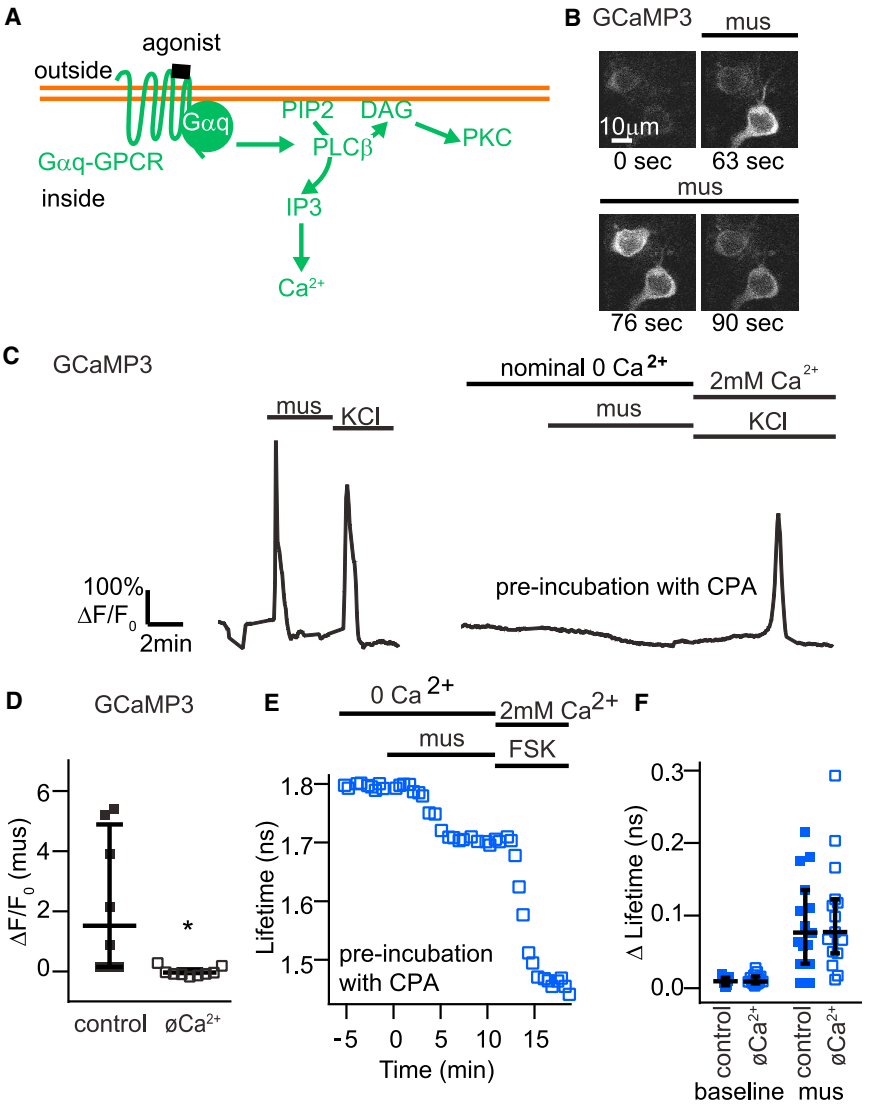

Figure 4. Calcium Transients Are Not Necessary for mAChR-Induced Net PKA Activation.

(A) Schematic illustrating model of Gαq signal transduction. Activation of Gαq-coupled receptors triggers PLCβ to cleave PIP2 into IP_3 and DAG. IP_3 activates IP_3 receptors, leading to Ca^{2+} release from intracellular stores. DAG or Ca^{2+} binds and activates PKC.

(B) Images of two GCaMP3-expressing hippocampal CA1 neurons showing fluorescence transients in response to bath application of mus in the reservoir at 0 s.

(C) Examples of GCaMP3 fluorescence changes in a CA1 pyramidal neuron in response to mus followed by 50 mM KCl application in control conditions (left) or in slices pre-incubated with 30 μM cyclopiazonic acid (CPA) and with nominal 0 Ca^{2+} ACSF (right).

(D) Summary of amplitudes of peak changes in GCaMP3 fluorescence in response to mus under control and treatment conditions (labeled as øCa^{2+}, corresponding to pre-incubation with CPA and using ACSF with nominal 0 Ca^{2+}). *$p < 0.05$ versus control.

(E) Time course of FLIM-AKAR lifetime changes in response to mus and FSK, with pre-incubation with CPA, and with nominal 0 Ca^{2+} in the ACSF.

(F) Summaries of FLIM-AKAR lifetime changes showing the effect of blocking Ca^{2+} transients on mus-induced PKA activity in the cytoplasm.

Each square represents a data point and black lines show median values with interquartile intervals. See also Figure S7 and Table S1.

et al., 2012; Yoshimasa et al., 1987), which is expressed in the hippocampus (Allen Developing Mouse Brain Atlas, 2008). To test whether AC2 can mediate PKC modulation of net PKA activity in our system, we transfected HEK cells with recombinant mouse *Adcy2*. FLIM-AKAR lifetime decreased in response to PDBu in *Adcy2*-transfected cells (Figure 5C; n = 4 for control cells, n = 11 for *Adcy2*-transfected cells, $p = 0.0015$ for control versus *Adcy2* for PDBu condition), showing that expression of *Adcy2* confers PKA modulation by PKC in HEK cells. Together, these experiments show that PKC is sufficient to increase net PKA activity in the hippocampus and suggest that *Adcy2* expression may account for the cell-type-specific regulation of PKA by PKC.

Since PKC activation is sufficient to increase net PKA activity in the hippocampus, we hypothesized that PKC is required for mAChR-induced phosphorylation by PKA. To test this, we applied the PKC inhibitor GF109203X (2 μM) to acute hippocampal slices. The inhibitor blocked PDBu-induced FLIM-AKAR phosphorylation (Figures S2I and S2J; n = 12, $p > 0.05$ for baseline versus PDBu). However, in the presence of the PKC inhibitor, mus induced a decrease in fluorescence lifetime that was larger than in control (Figures 5D, S7E, and S7F; n = 8 for control, n = 18 for GF109203X, $p = 0.0075$ for control versus GF109203X with mus). Together, these experiments show that activation of PKC is sufficient to increase PKA phosphorylation but is not required for mAChR-induced net PKA activation.

mAChR-Mediated Increase in Net PKA Activity Is Mediated by Parallel Signaling via Either Ca^{2+} Transients or PKC Activation

Since both Ca^{2+} transients and PKC activity are engaged in Gαq signaling, but neither is necessary for mAChR-mediated phosphorylation of FLIM-AKAR, we hypothesized that they had complementary roles. To test this hypothesis, we used conditions that blocked both Ca^{2+} transients and PKC activity. These conditions largely abolished mAChR-induced net PKA activation in the soma (Figures 6A, 6B, S7G, and S7H; n = 14 for control, n = 26 for GF and øCa^{2+}, $p < 0.0001$ for control versus GF and øCa^{2+} with mus), indicating that mAChR leads to net PKA activation via either PKC or Ca^{2+}. Notably, under these treatment

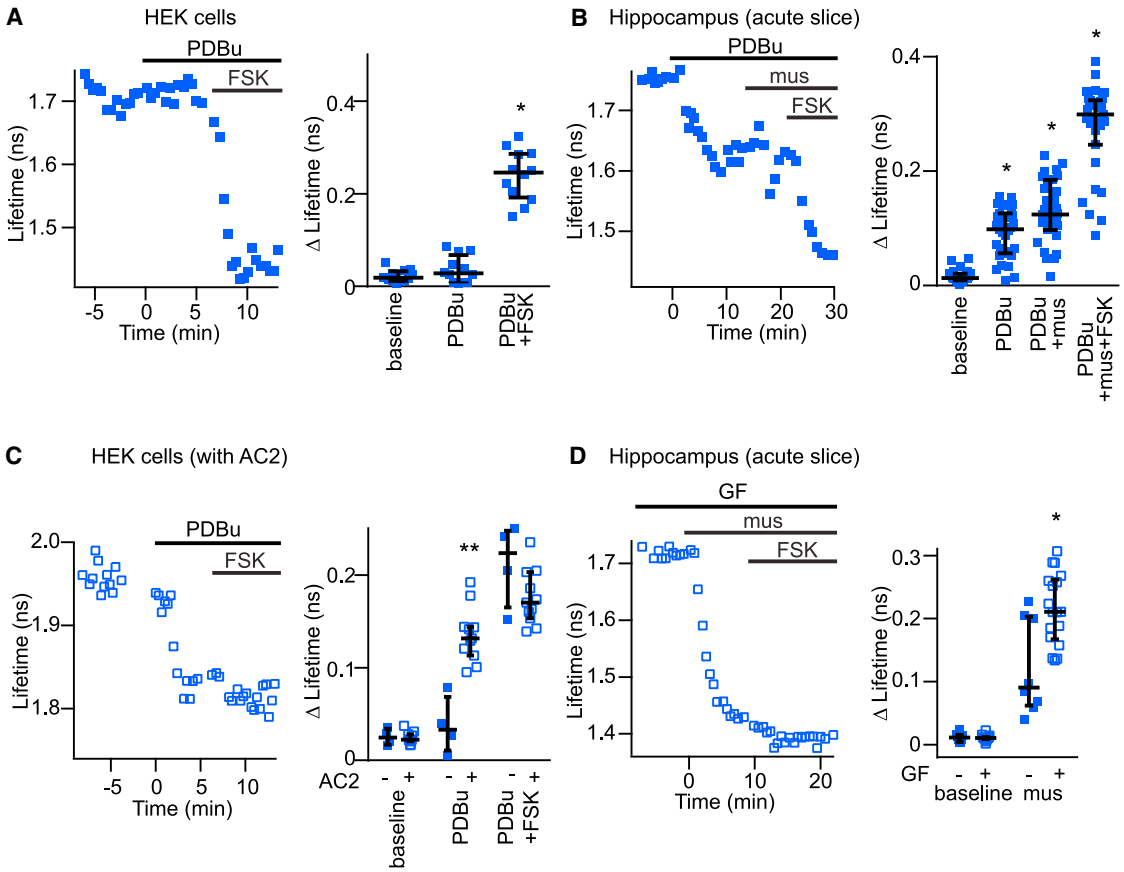

Figure 5. PKC Activation Is Sufficient, but Not Necessary, for mAChR-Induced Net PKA Activation

(A–C) Example time courses (left) and summaries (right) of FLIM-AKAR lifetime changes in response to the PKC activator phorbol 12, 13-dibutyrate (PDBu, 1 μM), and FSK, in HEK293 cells (A), acute hippocampal slices (B), and HEK293 cells transfected with adenylyl cyclase 2 (*Adcy2*) (C). *$p < 0.05$ versus baseline; **$p < 0.05$ versus AC2 negative cells.

(D) Example time course (left) and summaries (right) of FLIM-AKAR lifetime changes showing the effect of blocking PKC with the inhibitor GF109203X (GF, 2 μM). *$p < 0.05$ versus no GF.

Each square represents a data point and black lines show median values with interquartile intervals. See also Figures S2 and S7 and Table S1.

conditions, although mAChR-induced net PKA activation is largely abolished, activation of the Gαs-coupled β-adrenergic receptor with its agonist iso still decreased FLIM-AKAR lifetime (Figures 6C and S7I; n = 18, $p < 0.0001$ for baseline versus iso). These results, in addition to those with YM described above, demonstrate that net PKA activation does not simply occur due to non-specific coupling between mAChRs and Gαs; instead, Gαq- and Gαs-coupled receptors elevate net PKA activity through pharmacologically distinguishable mechanisms.

In summary, the results from mechanistic explorations reveal a pathway wherein Gαq-coupled mAChR activation increases net PKA activity via either PKC activation or Ca^{2+} transient (Figure 6D).

Multiple Gαq-Coupled Receptors Increase Net PKA Activity

Since Gαq induction of PKC activation and Ca^{2+} transients is not specific to mAChRs, we predicted that the unexpected signaling to a pathway normally associated with Gαs is a general feature of Gαq-coupled receptors. To test this prediction, we examined the effects of activating endogenous Gαq-coupled Group I metabotropic glutamate receptors (mGluRs) in hippocampal CA1 pyramidal neurons (Figure 7A). Activation with the Group I mGluR agonist DHPG (50 μM) significantly decreased FLIM-AKAR lifetime (Figures 7B, S8A, and S8B; n = 8, adjusted p = 0.047 for baseline versus DHPG), indicating that net PKA activation occurs downstream of multiple endogenous Gαq-coupled receptors.

In addition to endogenous receptors, we tested our prediction using hM3Dq, a widely used designer receptor exclusively activated by designer drugs (DREADD) that is Gαq coupled (Figure 7A) (Armbruster et al., 2007). Application of the ligand clozapine-N-oxide (CNO, 10 μM) induced net PKA activation in *hM3Dq*-transfected CA1 pyramidal neurons in acute hippocampal slices and occluded subsequent cytoplasmic mus response (Figures 7C, 7D, S8C, and S8D; n = 9, adjusted p = 0.012 for baseline versus CNO; p = 0.73 for CNO versus CNO+mus). Importantly, Gαq signaling is required for hM3Dq-induced increase in net PKA activity (Figures S8E and S8F; n = 9 for control,

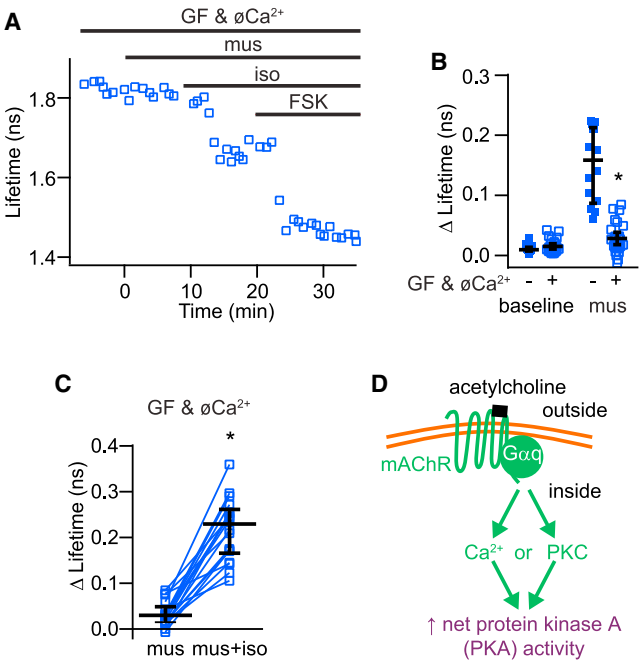

Figure 6. mAChR-Mediated Phosphorylation by PKA Is Mediated by Signaling via Either Ca^{2+} or PKC

(A) Example time courses of PKA activity reporter lifetime changes in response to mus and FSK with inhibition of both Ca^{2+} transients and PKC (nominal 0 Ca^{2+} in the external solution, pre-incubation with CPA and GF109203X, including GF109203X in the perfusing solution). Additional application of the Gαs-coupled β-adrenergic receptor agonist isoproterenol (iso, 1 μM) was used to assess whether net PKA modulation by Gαq- and Gαs-coupled receptors employ the same mechanism.

(B) Summaries of FLIM-AKAR lifetime changes showing the effect of blocking both Ca^{2+} transients and PKC activity on mus-induced PKA activity in the cytoplasm. *$p < 0.05$ versus control.

(C) Summary plots showing the amplitudes of FLIM-AKAR lifetime change in response to mus and subsequent addition of iso with inhibition of both Ca^{2+} transients and PKC. *$p < 0.05$ versus baseline.

(D) Model based on our data illustrating that Gαq-coupled mAChR activation increases net PKA activity via PKC or Ca^{2+} transient-dependent pathways.

Each square represents a data point and black lines show median values with interquartile intervals. See also Figure S7 and Table S1.

n = 10 for YM, p = 0.0003 for control versus YM with CNO), showing that the response is not due to ectopic Gαs coupling by the heterologous expression of hM3Dq. Finally, we also found that activation of hM3Dq increased PKA activity in a separate system (organotypic hippocampal slices) and with a separate reporter (the PSI reporter) (Figures S8G and S8H; n = 8, p = 0.0078 for baseline versus CNO). Thus, elevation of net PKA activity occurs with multiple Gαq-coupled receptors, including both endogenous receptors and those that are ectopically expressed.

DISCUSSION

Here, we study endogenous GPCRs in native brain tissue using optical reporters of PKA activation. We reveal the regulation by Gαq-coupled neuromodulator receptors of net PKA activity—the signal transduction effector classically associated with the Gαs and Gαi pathways (Figure 8). Mechanistically, the regulation is mediated via either PKC activation or Ca^{2+} transients. Furthermore, the findings generalize across multiple Gαq-coupled GPCRs, as evidenced by the net PKA response to activation of M1Rs, Group I mGluRs, and Gαq-coupled designer receptors. Together, these results show that one major family of GPCRs signal to the effector of another. Our results provide an important addition to the classical model of GPCR signaling and highlight PKA as an integrator of three major types of neuromodulator inputs (Gαs-, Gαi-, and Gαq-coupled receptors) in the brain.

Modulation of Net PKA Activity by Gαq-Coupled Neuromodulator Receptors

Although previous studies have implicated Gαq regulation of PKA, it was not possible to predict the directionality of the PKA response and thus the cellular function of a given Gαq-coupled receptor. Studies of GPCRs overexpressed in cell lines had demonstrated that Gαq-coupled receptors (e.g., M1Rs) can activate Gαq, Gαs, or Gαi signaling modules by coupling to each class of G protein (Burford and Nahorski, 1996; Felder et al., 1989; Peralta et al., 1988; Stein et al., 1988). Intracellularly, Ca^{2+} and PKC can have diverse effects on adenylyl cyclases, phosphodiesterases, phosphatases, and kinases, thereby potentially increasing or decreasing net PKA activity (Armstrong, 1989; Cooper et al., 1995; Geoffroy et al., 1999; Hunter et al., 2009; Lee et al., 1994; Lustig et al., 1993; Shen et al., 2012; Yoshimasa et al., 1987). This myriad of reports makes divergent and often conflicting predications about the potential of PKA modulation by Gαq-coupled receptors. Furthermore, many studies used overexpressed receptors or intracellular signaling components, likely introducing artifacts due to overexpression (Gibson et al., 2013). Finally, cellular signaling is highly spatiotemporally regulated (Gray et al., 1998; Lur and Higley, 2015; Tsvetanova and von Zastrow, 2014; Zhang et al., 2013), making it difficult to predict the effect of PKA regulation by an endogenous Gαq-coupled receptor in a specific brain region and cell type.

For these reasons, we monitored the time course of net PKA activity in individual cells in response to endogenous GPCR signaling in brain tissue, thereby revealing Gαq-GPCR modulation of net PKA activity in the brain regions and cells where they function. The importance of this approach is made clear here as the modulation of PKA by endogenous mAChRs in the hippocampus requires Gαq signaling (Figures 3C, 3D, S4C, and S4D), whereas that by overexpressed M1Rs in HEK293T cells does not (Figure S6), with the latter likely reflecting ectopic Gαs coupling of overexpressed M1Rs.

Since FLIM-AKAR reports phosphorylation of a PKA substrate, the increase in net PKA activity in response to Gαq activation could be due to an increase in PKA activity or a decrease in phosphatase activity. To distinguish these possibilities, we designed a second optical reporter (PSI) that reports the physical interaction between the catalytic subunit of PKAc and a PKA substrate (Figure 2G). Using PSI, we demonstrated enhanced PKAc/substrate interaction upon activation of mAChRs (Figures 2H and 2I). Thus, although we cannot rule out additional contributions of downregulation of phosphatase activity, the results from both optical reporters show that activation of mAChR increases PKA activity.

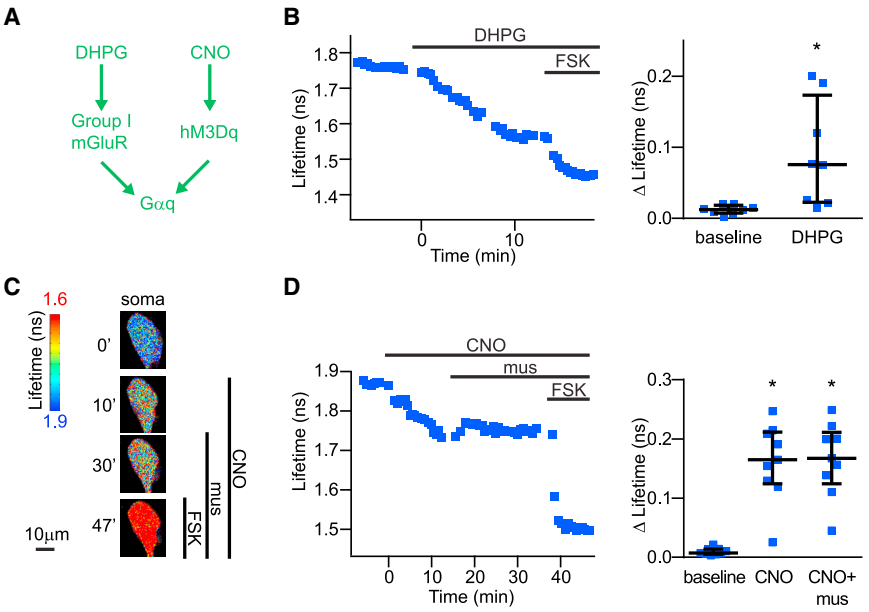

Figure 7. Gαq-Coupled Receptor Modulation of PKA Activity Occurs with Multiple Receptors

(A) Activation of Group I mGluRs by their agonist (S)-3,5-DHPG (DHPG) or activation of the designer receptor hM3Dqs by their agonist clozapine-N-oxide (CNO) leads to Gαq signaling.

(B) Example (left) and summary plot (right) showing response of FLIM-AKAR to DHPG (50 μM) and FSK in the cytoplasm of hippocampal CA1 pyramidal neurons. *$p < 0.05$ versus baseline.

(C) CNO (10 μM), an agonist of the Gαq-coupled designer receptor hM3Dq, increased net PKA activity in a CA1 pyramidal neurons expressing FLIM-AKAR and hM3Dq.

(D) Example plot (left) from the neuron in (C) and summaries (right) showing lifetime changes in the cytoplasm in response to CNO and subsequent application of mus and FSK. *$p < 0.05$ versus baseline.

Each square represents a data point and black lines show median values with interquartile intervals. See also Figure S8 and Table S1.

The FRET-FLIM based reporters can report PKA activity with subcellular spatial resolution and sub-second temporal precision (Chen et al., 2014) and thus provides additional spatiotemporal information on the PKA response to activation of Gαq. First, brief ACh application at specific dendritic branches with durations observed *in vivo* led to dendrite-specific and temporally transient net PKA activation (Figures 1F–1H and S1D). Second, the reporter revealed heterogeneity of responses across cells, and demonstrated Gαq-mediated reporter phosphorylation in the cytoplasm, nucleus, and dendrites (Figures 1 and S1). Third, real-time monitoring of net PKA activity showed a temporal delay of nuclear response compared with cytoplasm and dendrites (Figure 1I), likely due to the diffusion of cAMP, PKA, or phosphorylated PKA substrates such as the reporter from somatic cytoplasm into the nucleus (Chen et al., 2014). Finally, the reporter allowed us to observe acute responses to neuromodulator receptor stimulation, disambiguating between acute versus adaptive changes. These findings would be hard or impossible to capture with traditional biochemical methods that take a snapshot of the average response of a population of cells.

The Molecular Mechanisms of Gαq-GPCR Modulation of Net PKA Activity

We show that Gαq regulation of PKA can occur via either Ca^{2+} or PKC-dependent pathways. Previous work with overexpressed M1 receptors in CHO cells showed that M1Rs could couple directly to Gαs (Burford and Nahorski, 1996). This is unlikely to be the case in the hippocampus based on our data from two experiments. First, data with the Gαq inhibitor YM showed that Gαq signaling is required for mAChR-induced increase in PKA phosphorylation (Figures 3C, 3D, S4C, and S4D). Second, mAChR-mediated net PKA activity in the soma was abolished with concurrent inhibition of Ca^{2+} transients and PKC, whereas the Gαs-coupled beta-adrenergic response was still present (Figures 6C and S7I). Thus, the Gαs- and Gαq-coupled receptors employ pharmacologically distinguishable mechanisms to modulate net PKA activity in the hippocampus.

Any studies using biosensors and pharmacology require selectivity of the sensors and pharmacological reagents. We addressed the biosensor selectivity using two orthogonal sensors (FLIM-AKAR and PSI) (Figures 1 and 2G–2I), whose mechanisms of sensing are independent of each other. To dissect the intracellular mechanisms, we targeted multiple nodes of the Gαq-GPCR signaling pathway. We show that regulation of PKA by Gαq-mAChR requires (1) mAChR activity (Figures S2E–S2H), (2) Gαq signaling (Figures 3C, 3D, S4C, and S4D), (3) either Ca^{2+} transient or PKC activation (Figures 4, 5, 6, and S7), and (4) PKA activity (Figures 2 and S3). Although we cannot rule out complex contributions from other potential pathways, the preponderance of evidence indicates that the most parsimonious mechanism for Gαq-GPCR regulation of PKA activity is via bona fide Gαq signaling, mediated by either Ca^{2+} or PKC-dependent pathways.

The existence of multiple signaling pathways from GPCR activation to the same apparent outcome (i.e., enhanced phosphorylation by PKA) may provide several advantages. First, it may allow more precise spatiotemporal regulation of PKA activity. PKC-mediated mAChR regulation of PKA may, like Gαs/Gαi-dependent regulation (Lur and Higley, 2015; Zhang et al., 2013), be limited to signaling microdomains and thus highly compartmentalized. Ca^{2+}-mediated regulation of PKA, on the other hand, may lead to spatially broader cellular changes, since Ca^{2+} is released from intracellular stores into the cytoplasm, and not in a membrane-delineated fashion. Second, these pathways could cooperate to ensure the robustness of the response. Third, the existence of two pathways allows integration of a specific neuromodulator input with a wider range of other extracellular signals that impact the signaling components. Finally, these

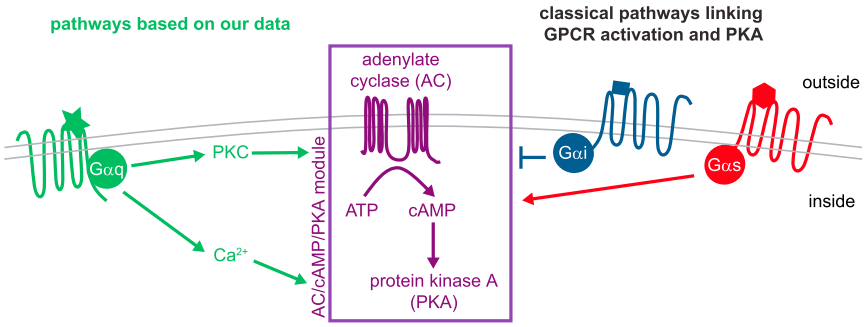

Figure 8. Revised Model of GPCR Modulation of Net PKA Activity

Classically, Gαs- and Gαi-coupled GPCRs stimulate and inhibit PKA activity respectively. Our data reveal an additional pathway wherein Gαq-coupled neuromodulator GPCR activation increases net PKA activity via PKC or Ca^{2+} transient-dependent pathways.

mechanisms predict the existence of positive and negative feedback loops. PKA activation can phosphorylate and modulate Ca^{2+} permeability of voltage-gated Ca^{2+} channels and NMDA receptors (Skeberdis et al., 2006; Vandael et al., 2013), and the resultant Ca^{2+} entry would in turn modulate both PKA and PKC activity (Cooper et al., 1995; Huang, 1989). PKC activation can also phosphorylate both adenylyl cyclase and phosphodiesterases (Geoffroy et al., 1999; Hunter et al., 2009; Lee et al., 1994; Lustig et al., 1993; Shen et al., 2012; Yoshimasa et al., 1987), which would increase and decrease PKA activity, respectively. Thus, these mechanisms could potentially generate complex transients of PKA activity in response to certain patterns of neuromodulator inputs.

The molecular mechanisms elucidated here help predict where and when Gαq-PKA signaling can occur. Since molecular components such as PLCβ and PKC are widely expressed, whether Gαq signals to PKA likely depends on the availability of specific ACs: AC2 for the PKC-mediated pathway and AC1/AC8/soluble adenylyl cyclase for the Ca^{2+}-mediated pathway (Cooper et al., 1995; Dunn et al., 2009). Differential distribution of ACs may act as a cellular or subcellular code to engage neither, one, or both arms of the Gαq pathway. This may explain, for example, why activation of the designer receptor hM3Dq increases PKA activity in the hippocampus (Figures 7C, 7D, and S8C–S8H), but not in COS7 or pancreatic β cells (Guettier et al., 2009). Thus, the cell-type specificity conferred by molecular components may explain seemingly conflicting observations and mechanisms across different cell lines and cell types (Bandrowski et al., 2001; Baumgold and Fishman, 1988; Onali and Olianas, 1990; Wang et al., 2008) and could give rise to functional specificity to Gαq signaling in different cell types and subcellular compartments.

Implications of Gαq-GPCR Modulation of Net PKA Activity

PKA phosphorylates many neurotransmitter receptors, ion channels, and transcription factors and is associated with synaptic plasticity (Esteban et al., 2003; Higley and Sabatini, 2010; Kandel and Abel, 1995; Lerner and Kreitzer, 2011; Seol et al., 2007; Shen et al., 2008; Skeberdis et al., 2006; Woolfrey and Dell'Acqua, 2015; Yasuda et al., 2003). Therefore, Gαq-mediated activation of net PKA activity has functional implications for a large family of GPCRs. For example, we showed that PKA activity is required for synaptic depression induced by the Gαq-coupled M1Rs (Figure S5). In addition, modulation of PKA by Gαq-coupled GPCRs likely explains previous biochemical findings such as the phosphorylation of GluA1 at the PKA phosphorylation site by M1R activation (Seol et al., 2007) and the regulation of Gαs signaling by Gαq-coupled receptors (Brown and Rietow, 1981; Cartmell et al., 1998; Enyedi et al., 1982; Goureau et al., 1990). Furthermore, Gαq-PKA coupling may contribute to multiple physiological and therapeutic processes, such as the mechanism of action for cholinergic drugs used to treat neuropsychiatric diseases (Higley and Picciotto, 2014; Thathiah and De Strooper, 2009) and amnesia induced by the mAChR antagonist scopolamine (Deutsch and Rocklin, 1967). Finally, this signaling pathway is likely conserved across species, as suggested by the mus-induced and PKA-dependent enhancement of stridulation in grasshoppers (Wenzel et al., 2002).

In addition to the explanatory value, the results of this study provide both practical and conceptual insights into the biology and experiments involving Gαq-coupled receptors. First, they inform the design and interpretation of experiments utilizing Gαq-coupled designer receptors, which will also engage PKA, a Gαs signaling effector, in specific cell types. Second, screening assays designed to identify ligands for orphan GPCRs suffer from a lack of knowledge in their G protein coupling and downstream signaling. The observation and molecular mechanisms elucidated here will allow investigators to engineer cell lines with the molecular components of the Gαq/PKA signaling and use them to deorphanize three major families of GPCRs with a single PKA activity assay. Third, modulation of net PKA activity is likely to be a general feature of Gαq-coupled neuromodulator receptors based on the mechanisms we have elucidated, and so the findings help predict cellular signaling and function for the large family of Gαq-coupled GPCRs. Finally, they reveal PKA as an integrator of cellular signaling from activation of the Gαs, Gαi, and Gαq-coupled neuromodulator receptors, adding an important branch to models of GPCR signaling and opening new directions of study on the integration of different classes of neuromodulators by PKA.

STAR★METHODS

Detailed methods are provided in the online version of this paper and include the following:

- KEY RESOURCES TABLE
- CONTACT FOR REAGENT AND RESOURCE SHARING

SUPPLEMENTAL INFORMATION

Supplemental Information includes eight figures and one table and can be found with this article online at https://doi.org/10.1016/j.neuron.2017.10.023.

AUTHOR CONTRIBUTIONS

Y.C. and B.L.S. designed the study. A.J.G., T.T., and A.K. collected and analyzed electrophysiology data. J.L.S. cultured organotypic slices and performed some *in utero* electroporation surgeries. Y.C. performed all the other experiments and analyzed the data. Y.C. and B.L.S. wrote the manuscript with critical comments from the other authors.

ACKNOWLEDGMENTS

The authors thank Haining Zhong, S. Dymecki, B. Lowell, K. Deisseroth, and M. During for plasmids; Arpiar Saunders for making the AAV-DFI-Gcamp3.8 plasmid; P. Jonak for assistance with development of image analysis code; Eli Lilly and Company for provision of the 77-LH-28-1 compound; Victoria Caldwell, Wagner Faria Messias, Jackie Birnbaum, and Lauren Chung for assistance; and Jonathan Cohen, Rafael Luna, and members of the Sabatini laboratory for critical comments on the manuscript. This work was supported by grants from the Nancy Lurie Marks Family Foundation (6193253-02 to B.L.S.), the Goldenson Fund (to Y.C.), and the NIH (R01NS046579 to B.L.S., F32DA035543 to Y.C., and P30NS072030 to the Neurobiology Imaging Facility).

Received: January 27, 2016
Revised: September 11, 2017
Accepted: October 16, 2017
Published: November 16, 2017

REFERENCES

Airan, R.D., Thompson, K.R., Fenno, L.E., Bernstein, H., and Deisseroth, K. (2009). Temporally precise in vivo control of intracellular signalling. Nature *458*, 1025–1029.

Allen, M.D., and Zhang, J. (2006). Subcellular dynamics of protein kinase A activity visualized by FRET-based reporters. Biochem. Biophys. Res. Commun. *348*, 716–721.

Allen Developing Mouse Brain Atlas (2008). Allen Developing Mouse Brain Atlas. http://developingmouse.brain-map.org/.

Armbruster, B.N., Li, X., Pausch, M.H., Herlitze, S., and Roth, B.L. (2007). Evolving the lock to fit the key to create a family of G protein-coupled receptors potently activated by an inert ligand. Proc. Natl. Acad. Sci. USA *104*, 5163–5168.

Armstrong, D.L. (1989). Calcium channel regulation by calcineurin, a Ca2+-activated phosphatase in mammalian brain. Trends Neurosci. *12*, 117–122.

Bandrowski, A.E., Ashe, J.H., and Crawford, C.A. (2001). Tetanic stimulation and metabotropic glutamate receptor agonists modify synaptic responses and protein kinase activity in rat auditory cortex. Brain Res. *894*, 218–232.

Baumgold, J., and Fishman, P.H. (1988). Muscarinic receptor-mediated increase in cAMP levels in SK-N-SH human neuroblastoma cells. Biochem. Biophys. Res. Commun. *154*, 1137–1143.

Berridge, M.J. (1983). Rapid accumulation of inositol trisphosphate reveals that agonists hydrolyse polyphosphoinositides instead of phosphatidylinositol. Biochem. J. *212*, 849–858.

Berridge, M.J., Dawson, R.M., Downes, C.P., Heslop, J.P., and Irvine, R.F. (1983). Changes in the levels of inositol phosphates after agonist-dependent hydrolysis of membrane phosphoinositides. Biochem. J. *212*, 473–482.

Brandon, E.P., Idzerda, R.L., and McKnight, G.S. (1997). PKA isoforms, neural pathways, and behaviour: Making the connection. Curr. Opin. Neurobiol. *7*, 397–403.

Brown, J.H., and Rietow, M. (1981). Muscarinic-dopaminergic synergism on retinal cyclic AMP formation. Brain Res. *215*, 388–392.

Burford, N.T., and Nahorski, S.R. (1996). Muscarinic m1 receptor-stimulated adenylate cyclase activity in Chinese hamster ovary cells is mediated by Gs alpha and is not a consequence of phosphoinositidase C activation. Biochem. J. *315*, 883–888.

Burford, N.T., Tobin, A.B., and Nahorski, S.R. (1995). Differential coupling of m1, m2 and m3 muscarinic receptor subtypes to inositol 1,4,5-trisphosphate and adenosine 3′,5′-cyclic monophosphate accumulation in Chinese hamster ovary cells. J. Pharmacol. Exp. Ther. *274*, 134–142.

Cardin, J.A., Carlén, M., Meletis, K., Knoblich, U., Zhang, F., Deisseroth, K., Tsai, L.H., and Moore, C.I. (2009). Driving fast-spiking cells induces gamma rhythm and controls sensory responses. Nature *459*, 663–667.

Carter, A.G., and Sabatini, B.L. (2004). State-dependent calcium signaling in dendritic spines of striatal medium spiny neurons. Neuron *44*, 483–493.

Cartmell, J., Goepfert, F., Knoflach, F., Pink, J.R., Bleuel, Z., Richards, J.G., Schaffhauser, H., Kemp, J.A., Wichmann, J., and Mutel, V. (1998). Effect of metabotropic glutamate receptor activation on receptor-mediated cyclic AMP responses in primary cultures of rat striatal neurones. Brain Res. *791*, 191–199.

Caulfield, M.P. (1993). Muscarinic receptors—characterization, coupling and function. Pharmacol. Ther. *58*, 319–379.

Chen, Y., Saulnier, J.L., Yellen, G., and Sabatini, B.L. (2014). A PKA activity sensor for quantitative analysis of endogenous GPCR signaling via 2-photon FRET-FLIM imaging. Front. Pharmacol. *5*, 56.

Cooper, D.M., Mons, N., and Karpen, J.W. (1995). Adenylyl cyclases and the interaction between calcium and cAMP signalling. Nature *374*, 421–424.

Dalton, G.D., and Dewey, W.L. (2006). Protein kinase inhibitor peptide (PKI): A family of endogenous neuropeptides that modulate neuronal cAMP-dependent protein kinase function. Neuropeptides *40*, 23–34.

Deutsch, J.A., and Rocklin, K.W. (1967). Amnesia induced by scopolamine and its temporal variations. Nature *216*, 89–90.

Dickinson, B.A., Jo, J., Seok, H., Son, G.H., Whitcomb, D.J., Davies, C.H., Sheng, M., Collingridge, G.L., and Cho, K. (2009). A novel mechanism of hippocampal LTD involving muscarinic receptor-triggered interactions between AMPARs, GRIP and liprin-alpha. Mol. Brain *2*, 18.

Drain, P., Folkers, E., and Quinn, W.G. (1991). cAMP-dependent protein kinase and the disruption of learning in transgenic flies. Neuron *6*, 71–82.

Dunn, T.A., and Feller, M.B. (2008). Imaging second messenger dynamics in developing neural circuits. Dev. Neurobiol. *68*, 835–844.

Dunn, T.A., Storm, D.R., and Feller, M.B. (2009). Calcium-dependent increases in protein kinase-A activity in mouse retinal ganglion cells are mediated by multiple adenylate cyclases. PLoS ONE *4*, e7877.

Enyedi, P., Fredholm, B.B., Lundberg, J.M., and Anggård, A. (1982). Carbachol potentiates the cyclic AMP-stimulating effect of VIP in cat submandibular gland. Eur. J. Pharmacol. *79*, 139–143.

Esteban, J.A., Shi, S.-H., Wilson, C., Nuriya, M., Huganir, R.L., and Malinow, R. (2003). PKA phosphorylation of AMPA receptor subunits controls synaptic trafficking underlying plasticity. Nat. Neurosci. *6*, 136–143.

Felder, C.C., Kanterman, R.Y., Ma, A.L., and Axelrod, J. (1989). A transfected m1 muscarinic acetylcholine receptor stimulates adenylate cyclase via phosphatidylinositol hydrolysis. J. Biol. Chem. *264*, 20356–20362.

Geoffroy, V., Fouque, F., Nivet, V., Clot, J.P., Lugnier, C., Desbuquois, B., and Benelli, C. (1999). Activation of a cGMP-stimulated cAMP phosphodiesterase by protein kinase C in a liver Golgi-endosomal fraction. Eur. J. Biochem. *259*, 892–900.

Gibson, T.J., Seiler, M., and Veitia, R.A. (2013). The transience of transient overexpression. Nat. Methods *10*, 715–721.

Gilman, A.G. (1995). Nobel Lecture. G proteins and regulation of adenylyl cyclase. Biosci. Rep. *15*, 65–97.

Goureau, O., Tanfin, Z., and Harbon, S. (1990). Prostaglandins and muscarinic agonists induce cyclic AMP attenuation by two distinct mechanisms in the pregnant-rat myometrium. Interaction between cyclic AMP and Ca2+ signals. Biochem. J. *271*, 667–673.

Gray, P.C., Scott, J.D., and Catterall, W.A. (1998). Regulation of ion channels by cAMP-dependent protein kinase and A-kinase anchoring proteins. Curr. Opin. Neurobiol. *8*, 330–334.

Greengard, P. (2001). The neurobiology of slow synaptic transmission. Science *294*, 1024–1030.

Guettier, J.-M., Gautam, D., Scarselli, M., Ruiz de Azua, I., Li, J.H., Rosemond, E., Ma, X., Gonzalez, F.J., Armbruster, B.N., Lu, H., et al. (2009). A chemical-genetic approach to study G protein regulation of beta cell function in vivo. Proc. Natl. Acad. Sci. USA *106*, 19197–19202.

Harvey, C.D., Yasuda, R., Zhong, H., and Svoboda, K. (2008). The spread of Ras activity triggered by activation of a single dendritic spine. Science *321*, 136–140.

Hasselmo, M.E. (2006). The role of acetylcholine in learning and memory. Curr. Opin. Neurobiol. *16*, 710–715.

Higley, M.J., and Picciotto, M.R. (2014). Neuromodulation by acetylcholine: Examples from schizophrenia and depression. Curr. Opin. Neurobiol. *29*, 88–95.

Higley, M.J., and Sabatini, B.L. (2010). Competitive regulation of synaptic Ca2+ influx by D2 dopamine and A2A adenosine receptors. Nat. Neurosci. *13*, 958–966.

Hokin, M.R., and Hokin, L.E. (1953). Enzyme secretion and the incorporation of P32 into phospholipides of pancreas slices. J. Biol. Chem. *203*, 967–977.

Huang, K.-P. (1989). The mechanism of protein kinase C activation. Trends Neurosci. *12*, 425–432.

Hulme, E.C., Birdsall, N.J.M., and Buckley, N.J. (1990). Muscarinic receptor subtypes. Annu. Rev. Pharmacol. Toxicol. *30*, 633–673.

Hunter, R.W., Mackintosh, C., and Hers, I. (2009). Protein kinase C-mediated phosphorylation and activation of PDE3A regulate cAMP levels in human platelets. J. Biol. Chem. *284*, 12339–12348.

Inoue, M., Kishimoto, A., Takai, Y., and Nishizuka, Y. (1977). Studies on a cyclic nucleotide-independent protein kinase and its proenzyme in mammalian tissues. II. Proenzyme and its activation by calcium-dependent protease from rat brain. J. Biol. Chem. *252*, 7610–7616.

Jo, J., Son, G.H., Winters, B.L., Kim, M.J., Whitcomb, D.J., Dickinson, B.A., Lee, Y.-B., Futai, K., Amici, M., Sheng, M., et al. (2010). Muscarinic receptors induce LTD of NMDAR EPSCs via a mechanism involving hippocalcin, AP2 and PSD-95. Nat. Neurosci. *13*, 1216–1224.

Kandel, E., and Abel, T. (1995). Neuropeptides, adenylyl cyclase, and memory storage. Science *268*, 825–826.

Kirk, C.J., Creba, J.A., Downes, C.P., and Michell, R.H. (1981). Hormone-stimulated metabolism of inositol lipids and its relationship to hepatic receptor function. Biochem. Soc. Trans. *9*, 377–379.

Krashes, M.J., Koda, S., Ye, C., Rogan, S.C., Adams, A.C., Cusher, D.S., Maratos-Flier, E., Roth, B.L., and Lowell, B.B. (2011). Rapid, reversible activation of AgRP neurons drives feeding behavior in mice. J. Clin. Invest. *121*, 1424–1428.

Langmead, C.J., Austin, N.E., Branch, C.L., Brown, J.T., Buchanan, K.A., Davies, C.H., Forbes, I.T., Fry, V.A., Hagan, J.J., Herdon, H.J., et al. (2008). Characterization of a CNS penetrant, selective M1 muscarinic receptor agonist, 77-LH-28-1. Br. J. Pharmacol. *154*, 1104–1115.

Lee, H.C., Cai, J.J., and Yu, H. (1994). Effect of protein kinase C on cyclic 3′, 5′-adenosine monophosphate-dependent phosphodiesterase in hypertrophic cardiomyopathic hamster hearts. J. Pharmacol. Exp. Ther. *270*, 1171–1176.

Lefkowitz, R.J. (2007). Seven transmembrane receptors: something old, something new. Acta Physiol. (Oxf.) *190*, 9–19.

Lennon, G., Auffray, C., Polymeropoulos, M., and Soares, M.B. (1996). The I.M.A.G.E. Consortium: an integrated molecular analysis of genomes and their expression. Genomics *33*, 151–152.

Lerner, T.N., and Kreitzer, A.C. (2011). Neuromodulatory control of striatal plasticity and behavior. Curr. Opin. Neurobiol. *21*, 322–327.

Levey, A.I., Edmunds, S.M., Koliatsos, V., Wiley, R.G., and Heilman, C.J. (1995). Expression of m1-m4 muscarinic acetylcholine receptor proteins in rat hippocampus and regulation by cholinergic innervation. J. Neurosci. *15*, 4077–4092.

Lu, W., Shi, Y., Jackson, A.C., Bjorgan, K., During, M.J., Sprengel, R., Seeburg, P.H., and Nicoll, R.A. (2009). Subunit composition of synaptic AMPA receptors revealed by a single-cell genetic approach. Neuron *62*, 254–268.

Lur, G., and Higley, M.J. (2015). Glutamate receptor modulation is restricted to synaptic microdomains. Cell Rep. *12*, 326–334.

Lustig, K.D., Conklin, B.R., Herzmark, P., Taussig, R., and Bourne, H.R. (1993). Type II adenylylcyclase integrates coincident signals from Gs, Gi, and Gq. J. Biol. Chem. *268*, 13900–13905.

Masuho, I., Ostrovskaya, O., Kramer, G.M., Jones, C.D., Xie, K., and Martemyanov, K.A. (2015). Distinct profiles of functional discrimination among G proteins determine the actions of G protein-coupled receptors. Sci. Signal. *8*, ra123–ra123.

Nishimura, A., Kitano, K., Takasaki, J., Taniguchi, M., Mizuno, N., Tago, K., Hakoshima, T., and Itoh, H. (2010). Structural basis for the specific inhibition of heterotrimeric Gq protein by a small molecule. Proc. Natl. Acad. Sci. USA *107*, 13666–13671.

Olianas, M.C., and Onali, P. (1992). Properties of muscarinic-stimulated adenylate cyclase activity in rat olfactory bulb. J. Neurochem. *58*, 1723–1729.

Onali, P., and Olianas, M.C. (1990). Positive coupling of cholinergic muscarinic receptors to adenylate cyclase activity in membranes of rat olfactory bulb. Naunyn Schmiedebergs Arch. Pharmacol. *342*, 107–109.

Parikh, V., Kozak, R., Martinez, V., and Sarter, M. (2007). Prefrontal acetylcholine release controls cue detection on multiple timescales. Neuron *56*, 141–154.

Peralta, E.G., Ashkenazi, A., Winslow, J.W., Ramachandran, J., and Capon, D.J. (1988). Differential regulation of PI hydrolysis and adenylyl cyclase by muscarinic receptor subtypes. Nature *334*, 434–437.

Pologruto, T.A., Sabatini, B.L., and Svoboda, K. (2003). ScanImage: flexible software for operating laser scanning microscopes. Biomed. Eng. Online *2*, 13.

Seol, G.H., Ziburkus, J., Huang, S., Song, L., Kim, I.T., Takamiya, K., Huganir, R.L., Lee, H.-K., and Kirkwood, A. (2007). Neuromodulators control the polarity of spike-timing-dependent synaptic plasticity. Neuron *55*, 919–929.

Shen, W., Flajolet, M., Greengard, P., and Surmeier, D.J. (2008). Dichotomous dopaminergic control of striatal synaptic plasticity. Science *321*, 848–851.

Shen, J.X., Wachten, S., Halls, M.L., Everett, K.L., and Cooper, D.M.F. (2012). Muscarinic receptors stimulate AC2 by novel phosphorylation sites, whereas

Gβγ subunits exert opposing effects depending on the G-protein source. Biochem. J. *447*, 393–405.

Skeberdis, V.A., Chevaleyre, V., Lau, C.G., Goldberg, J.H., Pettit, D.L., Suadicani, S.O., Lin, Y., Bennett, M.V., Yuste, R., Castillo, P.E., and Zukin, R.S. (2006). Protein kinase A regulates calcium permeability of NMDA receptors. Nat. Neurosci. *9*, 501–510.

Skoulakis, E.M., Kalderon, D., and Davis, R.L. (1993). Preferential expression in mushroom bodies of the catalytic subunit of protein kinase A and its role in learning and memory. Neuron *11*, 197–208.

Spangler, S.M., and Bruchas, M.R. (2017). Optogenetic approaches for dissecting neuromodulation and GPCR signaling in neural circuits. Curr. Opin. Pharmacol. *32*, 56–70.

Stein, R., Pinkas-Kramarski, R., and Sokolovsky, M. (1988). Cloned M1 muscarinic receptors mediate both adenylate cyclase inhibition and phosphoinositide turnover. EMBO J. *7*, 3031–3035.

Sternson, S.M., and Roth, B.L. (2014). Chemogenetic tools to interrogate brain functions. Annu. Rev. Neurosci. *37*, 387–407.

Stoppini, L., Buchs, P.A., and Muller, D. (1991). A simple method for organotypic cultures of nervous tissue. J. Neurosci. Methods *37*, 173–182.

Streb, H., Irvine, R.F., Berridge, M.J., and Schulz, I. (1983). Release of Ca2+ from a nonmitochondrial intracellular store in pancreatic acinar cells by inositol-1,4,5-trisphosphate. Nature *306*, 67–69.

Takai, Y., Yamamoto, M., Inoue, M., Kishimoto, A., and Nishizuka, Y. (1977). A proenzyme of cyclic nucleotide-independent protein kinase and its activation by calcium-dependent neutral protease from rat liver. Biochem. Biophys. Res. Commun. *77*, 542–550.

Thathiah, A., and De Strooper, B. (2009). G protein-coupled receptors, cholinergic dysfunction, and Abeta toxicity in Alzheimer's disease. Sci. Signal. *2*, re8.

Tian, L., Hires, S.A., Mao, T., Huber, D., Chiappe, M.E., Chalasani, S.H., Petreanu, L., Akerboom, J., McKinney, S.A., Schreiter, E.R., et al. (2009). Imaging neural activity in worms, flies and mice with improved GCaMP calcium indicators. Nat. Methods *6*, 875–881.

Tice, M.A., Hashemi, T., Taylor, L.A., and McQuade, R.D. (1996). Distribution of muscarinic receptor subtypes in rat brain from postnatal to old age. Brain Res. Dev. Brain Res. *92*, 70–76.

Tsvetanova, N.G., and von Zastrow, M. (2014). Spatial encoding of cyclic AMP signaling specificity by GPCR endocytosis. Nat. Chem. Biol. *10*, 1061–1065.

Vandael, D.H.F., Mahapatra, S., Calorio, C., Marcantoni, A., and Carbone, E. (2013). Cav1.3 and Cav1.2 channels of adrenal chromaffin cells: Emerging views on cAMP/cGMP-mediated phosphorylation and role in pacemaking. Biochim. Biophys. Acta *1828*, 1608–1618.

Vilaró, M.T., Palacios, J.M., and Mengod, G. (1990). Localization of m5 muscarinic receptor mRNA in rat brain examined by in situ hybridization histochemistry. Neurosci. Lett. *114*, 154–159.

Walsh, D.A., Ashby, C.D., Gonzalez, C., Calkins, D., and Fischer, E.H. (1971). Krebs EG: Purification and characterization of a protein inhibitor of adenosine 3′,5′-monophosphate-dependent protein kinases. J. Biol. Chem. *246*, 1977–1985.

Wang, H., Wu, L.-J., Zhang, F., and Zhuo, M. (2008). Roles of calcium-stimulated adenylyl cyclase and calmodulin-dependent protein kinase IV in the regulation of FMRP by group I metabotropic glutamate receptors. J. Neurosci. *28*, 4385–4397.

Wen, W., Meinkoth, J.L., Tsien, R.Y., and Taylor, S.S. (1995). Identification of a signal for rapid export of proteins from the nucleus. Cell *82*, 463–473.

Wenzel, B., Elsner, N., and Heinrich, R. (2002). mAChRs in the grasshopper brain mediate excitation by activation of the AC/PKA and the PLC second-messenger pathways. J. Neurophysiol. *87*, 876–888.

Wess, J. (2004). Muscarinic acetylcholine receptor knockout mice: Novel phenotypes and clinical implications. Annu. Rev. Pharmacol. Toxicol. *44*, 423–450.

Williams, J.T., Christie, M.J., and Manzoni, O. (2001). Cellular and synaptic adaptations mediating opioid dependence. Physiol. Rev. *81*, 299–343.

Woolfrey, K.M., and Dell'Acqua, M.L. (2015). Coordination of protein phosphorylation and dephosphorylation in synaptic plasticity. J. Biol. Chem. *290*, 28604–28612.

Yasuda, R. (2006). Imaging spatiotemporal dynamics of neuronal signaling using fluorescence resonance energy transfer and fluorescence lifetime imaging microscopy. Curr. Opin. Neurobiol. *16*, 551–561.

Yasuda, H., Barth, A.L., Stellwagen, D., and Malenka, R.C. (2003). A developmental switch in the signaling cascades for LTP induction. Nat. Neurosci. *6*, 15–16.

Yasuda, R., Harvey, C.D., Zhong, H., Sobczyk, A., van Aelst, L., and Svoboda, K. (2006). Supersensitive Ras activation in dendrites and spines revealed by two-photon fluorescence lifetime imaging. Nat. Neurosci. *9*, 283–291.

Yoshimasa, T., Sibley, D.R., Bouvier, M., Lefkowitz, R.J., and Caron, M.G. (1987). Cross-talk between cellular signalling pathways suggested by phorbol-ester-induced adenylate cyclase phosphorylation. Nature *327*, 67–70.

Zariwala, H.A., Borghuis, B.G., Hoogland, T.M., Madisen, L., Tian, L., De Zeeuw, C.I., Zeng, H., Looger, L.L., Svoboda, K., and Chen, T.-W. (2012). A Cre-dependent GCaMP3 reporter mouse for neuronal imaging in vivo. J. Neurosci. *32*, 3131–3141.

Zhang, M., Patriarchi, T., Stein, I.S., Qian, H., Matt, L., Nguyen, M., Xiang, Y.K., and Hell, J.W. (2013). Adenylyl cyclase anchoring by a kinase anchor protein AKAP5 (AKAP79/150) is important for postsynaptic β-adrenergic signaling. J. Biol. Chem. *288*, 17918–17931.

Zhong, H., Sia, G.M., Sato, T.R., Gray, N.W., Mao, T., Khuchua, Z., Huganir, R.L., and Svoboda, K. (2009). Subcellular dynamics of type II PKA in neurons. Neuron *62*, 363–374.

STAR★METHODS

KEY RESOURCES TABLE

REAGENT or RESOURCE	SOURCE	IDENTIFIER
Bacterial and Virus Strains		
AAV1-Cre-mCherry	Plasmid: Matthew During; Production: University of North Carolina Gene Therapy Center Virus Core Facility	N/A
AAV8-DFI-Gcamp3.8	Plasmid: Sabatini Lab; Production: University of North Carolina Gene Therapy Center Virus Core Facility	N/A
Chemicals, Peptides, and Recombinant Proteins		
ACh chloride	Sigma	Cat# A6625
(+)-mus-iodide	Tocris	Cat# 3074
forskolin	Tocris	Cat# 1099
isoproterenol	Tocris	Cat# 1747
Clozapine N-oxide	Tocris	Cat# 4936
Scopolamine hydrobromide	Tocris	Cat# 1414
Cyclopiazonic acid	Tocris	Cat# 1235
Phorbol 12,13-dibutyrate	Tocris	Cat# 4153
GF 109203X	Tocris	Cat# 0741
(S)-3,5-DHPG	Tocris	Cat# 0805
DPCPX	Tocris	Cat# 0439
picrotoxin	Tocris	Cat# 1128
NBQX	Tocris	Cat# 0373
(R)-CPP	Tocris	Cat# 0247
PKI 14-22 amide, myristoylated	Tocris	Cat# 2546
Tetrodotoxin citrate	Abcam	Cat# ab120055
Tetrodotoxin citrate	Tocris	Cat# 1069
YM-254890	Wako	Cat# 257-00631
77-LH-28-1	Eli Lilly and company	N/A
Experimental Models: Cell Lines		
Human: HEK293T cells	ATCC	CRL-3216
Experimental Models: Organisms/Strains		
Mouse: C57BL/6NCrl	Charles River	Cat# 027; RRID: IMSR_CRL:27
Mouse: B6.Cg-*Gt(ROSA)26Sor*$^{tm38(CAG-GCaMP3)Hze}$/J	Jackson Laboratory	Cat# 029043; RRID: IMSR_JAX:014538;
Rat: CD IGS Sprague Dawley	Charles River	Cat# 001
Recombinant DNA		
AAV-FLIM-AKAR	(Chen et al., 2014)	Addgene# 63058
AAV-FLEX-FLIM-AKAR	(Chen et al., 2014)	Addgene# 60445
AAV-FLEX-FLIM-AKAR^{T391A}	(Chen et al., 2014)	Addgene# 60466
AAV-FLEX-PKIα-IRES-mRuby2	(Chen et al., 2014)	Addgene# 63059
pCMV-SPORT6-adcy2	(Lennon et al., 1996)	Invitrogen IMAGE: 5367175
pcDNA3.1-human M1R	cDNA Resource Center	Cat# MAR0100000
pCAGGSS-mouse PKA-Calpha-mEGFP	(Zhong et al., 2009)	Addgene# 45528
pBS-β-actin-Cre	Susan Dymecki	N/A
AAV-DIO-hM3Dq-mCherry	(Krashes et al., 2011)	N/A
mCherry-tagged PKA consensus substrate	This paper	Will be deposited to Addgene

(*Continued on next page*)

Continued

REAGENT or RESOURCE	SOURCE	IDENTIFIER
Software and Algorithms		
MATLAB	MathWorks	RRID: SCR_001622
ScanImage	(Pologruto et al., 2003)	https://github.com/bernardosabatinilab/SabalabSoftware_Nov2009
GraphPad Prism 7	GraphPad Software	RRID: SCR_002798

CONTACT FOR REAGENT AND RESOURCE SHARING

Further information and requests for resources and reagents should be directed to and will be fulfilled by the Lead Contact, Bernardo Sabatini (bernardo_sabatini@hms.harvard.edu).

EXPERIMENTAL MODEL AND SUBJECT DETAILS

HEK293T Cells

HEK293T cells (Invitrogen) were cultured in DMEM with 10% FBS, sodium pyruvate (1 mM), L-glutamine (2 mM), and penicillin (50 U/ml) /streptavidin (50 μg/ml) (all reagents from GIBCO) at 37°C in 5% CO_2. The gender of the cells is female. The cell line has not been authenticated. They were used as a non-neuronal cell line to verify that FLIM-AKAR was not directly phosphorylated by PKC, and were not tested for mycoplasma. They were plated on coverslips in 24-well plates and transfected with the plasmid AAV-FLIM-AKAR, AAV-FLIM-AKAR and mouse adcy2, or AAV-FLIM-AKAR and pcDNA3.1-human M1R using Lipofectamine 2000 (Invitrogen). One or two days after transfection, the cells were imaged in solutions containing either HEPES-based buffer (containing in mM: 130 KCl, 1 EGTA, 1 $MgCl_2$, 25 HEPES, 10 glucose, 20 sucrose, pH with KOH to 7.4) or ACSF (see below).

Animals

All procedures for rodent husbandry and surgery were performed following protocols approved by the Harvard Standing Committee on Animal Care and in accordance with National Institutes of Health guidelines. C57BL/6 wild-type mice (Charles River) between postnatal days 15 and 19 (P15-P19) were used for PKA imaging experiments and for Ca^{2+} imaging experiments in Figures S2C and S2D, and mice at P21-P28 were used for Figure S5. For Ca^{2+} imaging experiments in Figure 4, the Ai38 mouse with $GCaMP3^{f/f}$ genotype (Tian et al., 2009; Zariwala et al., 2012) (MGI: 5014745; RRID: IMSR_JAX:014538) at age P27-P38 were used. Both male and female mice were used.

Since we observed a bigger mus-induced increase in net PKA activity with enriched environment, all experiments with FLIM imaging of the PKA reporter were performed following environment enrichment. This involves transfer of animals at P4-P7 to a larger cage that contained a shack, 3-4 pieces of nestlets, a tunnel, a hut, a running wheel, and a novel toy, as well as embedded yogurt drops in the bedding. To maximize novelty exposure of the animals, the hut, wheel, and novel toy were replaced with the same types of objects, but with different colors and shapes every other day. Fresh yogurt drops were also embedded in the bedding every other day.

Organotypic Hippocampal Cultures

For the experiments in Figures S8G and S8H, organotypic hippocampal slices were cultured from 7 days old Spraque Dawley rats (Stoppini et al., 1991). Both male and female rats were used. The brain was dissected and immediately placed in cold dissection media. Transverse hippocampal slices were cut with 400 μm thickness and placed above a sterile culture insert (Millicell-CM, Millipore) in 6-well plates containing prewarmed culture media. DNA plasmids were biolistically transfected with a Helios Gene Gun (Biorad) 5-7 days after culturing, and the slice were imaged 3-4 days after transfection.

METHOD DETAILS

DNA Plasmids

The constructs AAV-FLIM-AKAR, AAV-FLEX-FLIM-AKAR, AAV-FLEX-FLIM-$AKAR^{T391A}$ and AAV-FLEX-PKIα-IRES-mRuby2 were described in Chen et al. (2014) (Addgene #s 63058, 60445, 60466 and 63059). pCMV-SPORT6-adcy2 was an IMAGE clone from Invitrogen (IMAGE: 5367175; Lennon et al., 1996). pcDNA3.1-human M1R was from cDNA Resource Center (http://www.cdna.org/home.php?cat=0). PKAc-mEGFP (pCAGGSS-mouse PKA-Calpha-mEGFP) was a gift from Haining Zhong (Addgene # 45528) (Zhong et al., 2009). pBS-β-actin-Cre was a gift from Susan Dymecki at Harvard Medical School. The Gq-DREADD hM3Dq construct (AAV-DIO-hM3Dq-mCherry) was a gift from Brad Lowell at Beth Israel Deaconess Medical Center (Armbruster et al., 2007; Krashes

et al., 2011). The AAV-Cre-mCherry construct was from Matthew During at Ohio State University. AAV-DFI-Gcamp3.8 was cloned by replacing ChR2-mCherry in AAV-EF1α-DFI-ChR2-mCherry (Cardin et al., 2009) with Gcamp3.8.

For the construction of the mCherry-tagged PKA consensus substrate, the mEGFP and sReaCh regions of AAV-FLEX-FLIM-AKAR were each replaced by mCherry through gene synthesis and subcloning via ApaI and BglII sites. Subsequently, site-directed mutagenesis was performed to mutate the threonine to alanine at the phosphorylation site of the consensus substrate (Genscript).

In Utero Electroporation

In utero electroporation was used to deliver plasmids as described previously (Chen et al., 2014). During electroporation, the embryo head was held with a tweezertrode (5mm electrode diameter, Harvard Apparatus) and electric pulses were delivered five times (50 V, 50 ms pulse with 950ms interval) for hippocampus delivery of DNA (CUY21 electroporator, NEPA GENE, Japan).

Virus Production and Stereotaxic Injections

For GCaMP3 imaging, AAV1-Cre-mCherry and AAV8-DFI-Gcamp3.8 were packaged at University of North Carolina Gene Therapy Center Virus Core Facility. For Figures 4B–4D, P16-P21 pups with the genotype GCaMP3$^{f/f}$ were anesthetized with isofluorane and placed on a small stereotaxic frame (David Kopf Instruments). To target the hippocampus, coordinates of posterior 2.8 mm and lateral 3.0 mm relative to Bregma, 2.2 mm from the pia were used. Unilateral injections of 1 μL of AAV1-Cre-mCherry (2×10^{12} genome copy/ml) were made into the right hemispheres at a rate of 100 nl/min through a UMP3 micro syringe pump (World Precision Instruments). After injection, pups were returned to their home cage with their mother, weaned around P21-P23, and expression was allowed to occur for at least 11 days post infection. For Figures S2C and S2D, AAV1-Cre-mCherry (2×10^{12} genome copy/ml) and AAV-DFI-Gcamp3.8 ($1.39X10^{12}$ virus molecules/ml) were injected into P0/P1 hippocampus according to previously published procedures (Lu et al., 2009), and mice were imaged at P15-P19.

Brain Slice Preparation

Mice were anesthetized with isoflurane before being sacrificed. Their brains were rapidly dissected out.

For all the experiments except for those in Figures S5, S8G, and S8H, acute horizontal sections were sliced from the hippocampus with a Leica VT1000S vibratome (Leica Instruments) in cold sucrose cutting solution (containing in mM: 87 NaCl, 25 NaHCO3, 1.25 NaH2PO4 2.5 KCl, 75 sucrose, 25 glucose, 7.5 MgCl2). Slices were 300 μm thick. After sectioning, slices were transferred to ACSF (containing in mM: 127 NaCl, 2.5 KCl, 25 $NaHCO_3$, 1.25 NaH_2PO_4, 2 $CaCl_2$, 1 $MgCl_2$, and 25 glucose; for nominal 0 Ca^{2+} experiments, ACSF contained no $CaCl_2$ and 3 $MgCl_2$). The slices were incubated for recovery at 34°C for 5-10 minutes (imaging experiments) or 30 minutes (electrophysiology recordings), and then kept in ACSF at room temperature. Slices were then transferred to a microscope chamber and ACSF was perfused at a flow rate of 2–4 ml/min.

For the experiments in Figure S5, acute visual cortical slices (300 μm) were prepared as described (Seol et al., 2007). Briefly, slices were sectioned in ice-cold cutting buffer (containing in mM: 212.7 sucrose, 5 KCl, 1.25 NaH_2PO_4, 10 $MgCl_2$, 0.5 $CaCl_2$, 26 $NaHCO_3$, 10 dextrose). The slices were transferred to ACSF (containing in mM: 124 NaCl, 5 KCl, 1.25 NaH_2PO_4, 1 $MgCl_2$, 2 $CaCl_2$, 26 $NaHCO_3$, 10 dextrose) for recovery at 30°C for 30 minutes then at room temperature for at least 30 minutes prior to recording.

All solutions were continuously bubbled with carbogen (95% O2, 5% CO2), and the experiments were performed at 30°C-34°C.

Slice Processing and Microscopy with a Slide Scanner

For images in Figure 1B, mice were deeply anesthetized at P30 with isoflurane and perfused transcardially with 4% paraformaldehyde in phosphate buffered saline (PBS). Brains were post-fixed overnight, washed in PBS and 40 μm parasagittal sections were cut with a Leica VT1000S vibratome (Leica Instruments). They were then mounted on superfrost slides, dried and covered with ProLong antifade reagent containing DAPI (Molecular Probes) followed by a coverslip. Whole sections were imaged with an Olympus VS120 slide-scanning microscope.

Two-photon Imaging of Ca^{2+} Signals and 2pFLIM

Two photon imaging was achieved by a custom-built microscope with a mode-locked Ti-sappire laser source (Carter and Sabatini, 2004; Chen et al., 2014) (Chameleon Vision II, 80 MHz, Coherent). Photons were collected with fast photomultipler tubes (PMTs) (H7422-40MOD, Hamamatsu). A 60X (NA1.1) objective (Olympus) was used. Image acquisition was performed using a custom-written software ScanImage that ran in MATLAB (Chen et al., 2014; Pologruto et al., 2003).

For Ca^{2+} imaging, 910nm was used as the excitation wavelength, and 128x128 pixel images were collected by frame scan at 4Hz. CA1 neurons with basal GCaMP3 signals excluded from the nucleus were used for experiments since neurons with labeled nuclei were previously shown to have impaired calcium homeostasis and GCaMP3 function (Tian et al., 2009). At the end of all Ca^{2+} imaging experiments, 50mM KCl was applied to activate voltage-gated calcium channels as a positive control for cell health.

FLIM was performed as described previously (Chen et al., 2014). The FLIM board SPC-150 (Becker and Hickl GmbH) was used, and time-domain single photon counting was performed in 256 time channels. 920nm excitation wavelength was used to excite the donor fluorophore mEGFP in FLIM-AKAR.

Figure 1F was constructed from the maximum projections along the z dimension of two regions of interests acquired with a two-photon microscope, at 3 frames per z slice and 1 μm per z step. All experiments were performed in the presence of 1 μM DPCPX to inhibit adenosine receptors, and 1 μM tetrodotoxin to block action potentials.

Ca^{2+} Image Analysis

Each region of interest (ROI) corresponding to a single neuronal cell body was manually selected. The fluorescence signal for all pixels in a given ROI was averaged and plotted against time. The $\Delta F/F_0$ was calculated as $(F-F_0)/F_0$, where F_0 is the fluorescence signal averaged over the entire baseline period (usually 2.5-3 minutes).

FLIM Image Analysis

Fluorescence lifetime curve fitting and the calculation of average lifetime over a particular region of interest were performed as described previously (Chen et al., 2014; Harvey et al., 2008; Yasuda et al., 2006). Instrument response curve (IRF) was measured with double harmonic generation of urea crystals and used to deconvolve the fluorescence decay curve. The time constant for the free donor lifetime (τ_{free}) was determined by transfecting the donor alone into HEK293T cells, and was determined to be 2.14ns. To determine the time constant for donors that have undergone FRET (τ_{FRET}), FLIM-AKAR was transfected into HEK293T cells, and the best double exponential fit was performed with τ_{free} fixed at 2.14ns. τ_{FRET} was determined to be 0.69ns. These values of τ_{free} and τ_{FRET} were then used for double exponential fitting of lifetime distribution curves during all experiments.

Only images with photon count rates between 40,000 photons per second (40KHz) and 1.3MHz were used. The lower limit ensures accurate lifetime estimation based on our simulation, and gives a standard deviation of lifetime estimate of 0.0035ns. The upper limit ensures that we do not run into dead time and pile-up issues of the FLIM board.

For ROI analysis, somatic cytoplasm, nucleus and dendrite were segmented via a semi-automated software written in MATLAB that utilizes both intensity and lifetime data. The image segmentation was visually inspected and revised by the experimenter post automation.

The amplitudes of lifetime changes were quantitated as follows (Figure S1A):

$$\begin{gathered}\text{BaselineStart} = \text{lifetime measurements averaged over the first minute of baseline;}\\ \text{BaselineEnd} = \text{lifetime measurements averaged over the last minute of baseline;}\\ \text{BaselineMin} = \text{minimum lifetime measurement during baseline;}\\ \text{TreatmentMin} = \text{minimum lifetime measurement after a particular drug flow} - \text{in, before the next drug flow in.}\\ \Delta\text{lifetime (baseline)} = \text{BaselineMin} - \text{BaselineStart;}\\ \Delta\text{lifetime (Treatment)} = \text{TreatmentMin} - \text{BaselineEnd.}\end{gathered}$$

Electrophysiology

For Figure S3B, paired whole-cell voltage clamp recordings were taken from transfected hippocampal CA1 pyramidal neurons, identified by mRuby2 epifluorescence for PKIα-IRES-mRuby2 expressing cells, and neighboring untransfected control cells. Slices were perfused in ACSF containing 100 μM picrotoxin. Results from two conditions (10 μM NBQX or 10 μM (R)-CPP) were pooled for analysis. Whole-cell access to recorded neurons was made using 3-5 MΩ glass pipettes filled with internal solution containing (in mM): 135 CsMeSO4, 8 NaCl, 10 HEPES, 0.3 EGTA, 5 QX-314, 4 Mg-ATP, 0.3 Na-GTP, 0.1 spermine, at 293 mOsm and pH 7.24. Voltage-clamp was performed using a Multiclamp 700B amplifier (Molecular Devices) with a 3 KHz Bessel filter, digitized at 10 KHz using a National Instruments data acquisition board, and recorded and analyzed using ScanImage. Input resistance and capacitance were calculated following whole-cell break-in by fitting a 5 mV test pulse with an exponential decay, and holding current measured when neurons were voltage-clamped to −70 mV.

For Figure S5, visualized whole-cell current-clamp recordings were made from layer II/III regular-spiking pyramidal cells using MultiClamp 700A amplifier (Molecular Devices). Borosillicate glass recording pipettes (4-6 MΩ) were filled with intracellular solution containing (in mM): 130 K-Gluconate, 10 KCl, 0.2 EGTA, 10 HEPES, 4 Mg-ATP, 0.5 Na-GTP, 10 Na-Phosphocreatine, with or without 0.01 myristoylated PKI 14-22 amide, at 280-290mOsm and pH 7.25. Only cells with membrane potentials more negative than −65 mV, series resistance < 20 MΩ (8-18 MΩ, compensated at 80%), and input resistance larger than 100 MΩ were studied. Cells were excluded if input resistance changed > 15% over the entire experiment, with the exception of changes during bath application of the agonists. Data were filtered at 2 kHz and digitized at 5 kHz using Igor Pro (WaveMetrics Lake Oswego, Oregon). Synaptic responses were evoked every 15 s by stimulating layer IV with 0.2 ms pulses delivered through theta glass pipettes filled with ACSF. Intensity was adjusted to evoke a 4-6 mV response. Synaptic strength was quantified as the initial slope (the first 2 ms) of the EPSP. One cell per slice was used.

Pharmacology

Unless otherwise noted, all chemicals were applied via bath perfusion: they were either spiked into the perfusion reservoir, or pre-made buffers with the specified chemical concentrations were switched from one to another via a custom-made solution exchanger. Lifetime was allowed to stabilize before a new chemical was added; when there was no clear lifetime changes, 10 minutes were given

before the addition of another chemical. Whenever possible, perturbation experiments were performed with interleaved brain slices, and the perfusion tubing was washed and changed for different drug conditions. The final concentrations of chemicals are specified in brackets: ACh (100 μM) was from Sigma; (+)-mus-iodide (10 μM), forskolin (50 μM), isoproterenol (1 μM), clozapine N-oxide (10 μM), scopolamine hydrobromide (10 μM), cyclopiazonic acid (30 μM, pre-incubation at room temperature for at least 35 minutes), phorbol 12, 13-dibutyrate (1 μM), GF 109203X (2 μM, and pre-incubation at room temperature for at least 35 minutes), (S)-3,5-DHPG (50 μM), DPCPX (1 μM), picrotoxin (100 μM), NBQX (10 μM) and (R)-CPP (10 μM), PKI 14-22 amide, myristoylated (10 μM, included in the internal solution in the patch pipette) were from Tocris Bioscience; tetrodotoxin citrate (1 μM) was from Abcam and Tocris; YM-254890 (1 μM, and pre-incubation at 32°C for at least 10 minutes) was from Wako; and 77-LH-28-1 (10 μM) was a gift from Eli Lilly and company.

For ACh puffing experiments, ACh (200 μM in ACSF) was puffed onto an apical or basal dendrite from a glass patch pipette via a picospritzer (Parker) at 2 psi, and approximately 30 μm from the dendrite.

QUANTIFICATION AND STATISTICAL ANALYSIS

Detailed information of sample descriptions and statistics can be found in Table S1, and was also summarized in the Figure Legends, Figures, and Results. All statistical analyses were performed in GraphPad Prism.

Sample size n reported here refers to biological replicates of number of neurons. Figure S5C shows mean ± standard error of the mean (SEM). In all the other figures, each square represents a data point, black lines show median values with interquartile intervals.

Nonparametric two-tailed tests were used for all statistical analyses. For comparison between before and after drug application, and for comparison with paired electrophysiology recordings between PKI negative and positive neurons, Wilcoxon matched pairs signed rank test was used. For comparison between different treatment conditions, Mann Whitney test was used. For data in Figure S5, the last 2.5 minutes of baseline or agonist application were averaged and used for statistical comparison. To ask if PKA activity is modulated by non-mAChR receptors that are Gαq coupled, Bonferroni correction was used to counteract the problem of multiple comparisons for more than one GPCR.

For experiments with mus, sample distributions in Figure 1J were used for power calculation to determine sample size. For the other experiments, standard replicate numbers in the field were used.

DATA AND SOFTWARE AVAILABILITY

The MATLAB programs for ScanImage for data acquisition and analysis are available at https://github.com/bernardosabatinilab/SabalabSoftware_Nov2009. All other code is available upon request. The summary statistics of all the data are can be found in Table S1.